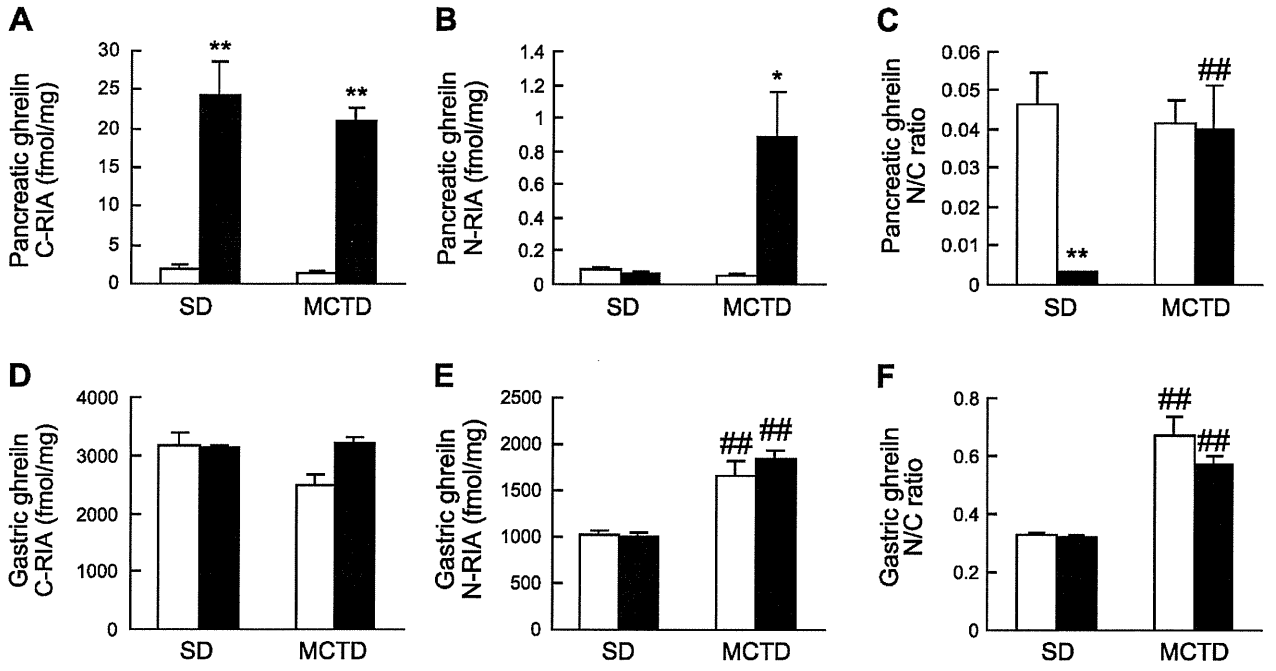

Fig. 2. Pancreatic and gastric ghrelin levels in RIP-GG Tg mice on standard (SD) or medium-chain triglyceride-rich diet (MCTD). *A* and *B*: pancreatic ghrelin levels in RIP-GG Tg mice (black bars) and nontransgenic controls (open bars) measured by using anti-ghrelin [13–28] (C-RIA; *A*) and anti-ghrelin [1–11] (N-RIA; *B*). Although total ghrelin levels measured by C-RIA were elevated in RIP-GG Tg mice on both SD and MCTD, ghrelin levels measured by N-RIA were elevated only when RIP-GG Tg mice were fed MCTD. *D* and *E*: gastric ghrelin levels of RIP-GG Tg mice (black bars) and nontransgenic controls (open bars) measured by C-RIA (*D*) or N-RIA (*E*) were significantly higher than pancreatic levels, regardless of diet. *C* and *F*: The ratio of N-RIA/C-RIA (N/C). $^{**}P < 0.01$ and $^{*}P < 0.05$ compared with controls. $\#\#P < 0.01$ compared with SD; $n = 5–7$.

We measured plasma ghrelin levels in the portal veins of RIP-GG Tg mice fed a MCTD to determine whether this level of ghrelin overexpression in islets could affect plasma ghrelin levels. No significant changes were observed in either ghrelin or desacyl ghrelin levels in the portal veins of RIP-GG Tg mice (Fig. 4, *A* and *B*), indicating that ghrelin overexpression from the transgene in islets produces minimal effect on plasma ghrelin levels.

Glucose metabolism and insulin secretion in RIP-GG Tg mice. No significant changes in blood glucose levels were seen by intraperitoneal glucose tolerance tests between 10-wk-old RIP-GG Tg mice and controls on a MCTD (Fig. 5*A*). Plasma insulin levels before and after a glucose load were not altered significantly in 15-wk-old RIP-GG Tg mice on a MCTD (Fig. 5*B*). There were also no significant changes in blood glucose or plasma insulin levels after glucose load in old mice (≈84-wk old) or in female mice (Fig. 5, *C–F*).

Islet architecture. There were no obvious abnormalities in intraislet cytoarchitecture or in the cell numbers of insulin-, glucagon-, somatostatin-, and polypeptide-producing cells in the islets of RIP-GG Tg mice on MCTD (Fig. 6, *A–D*).

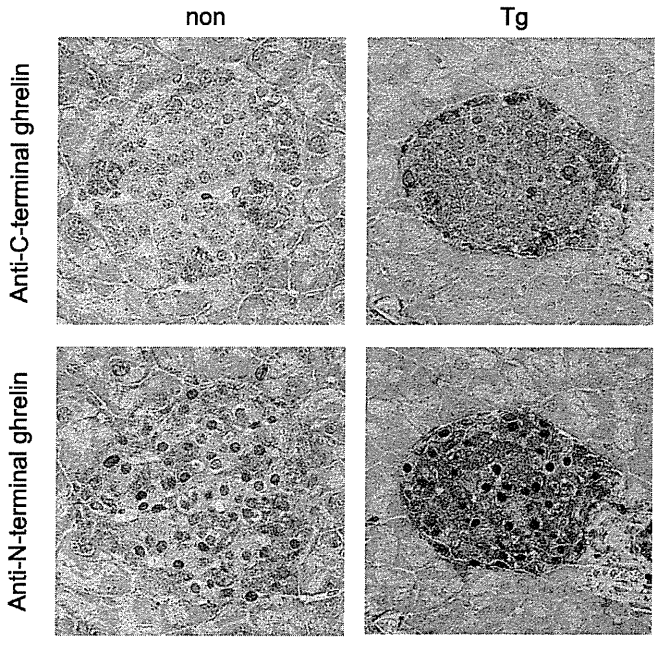

Fig. 3. Immunohistochemical analysis of the expression of ghrelin in the islets of RIP-GG Tg mice. Ghrelin-like immunoreactivities were increased in the core of the islets of RIP-GG Tg mice on MCTD.

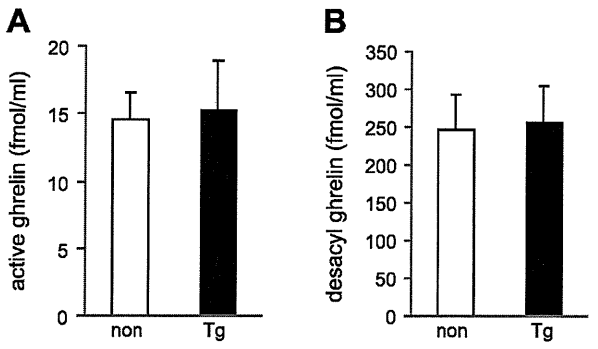

Fig. 4. Portal ghrelin levels of RIP-GG Tg mice. *A* and *B*: portal ghrelin (*A*) and desacyl ghrelin levels (*B*) in male Tg (black bars) and non (open bars) fed MCTD; $n = 7–8$.

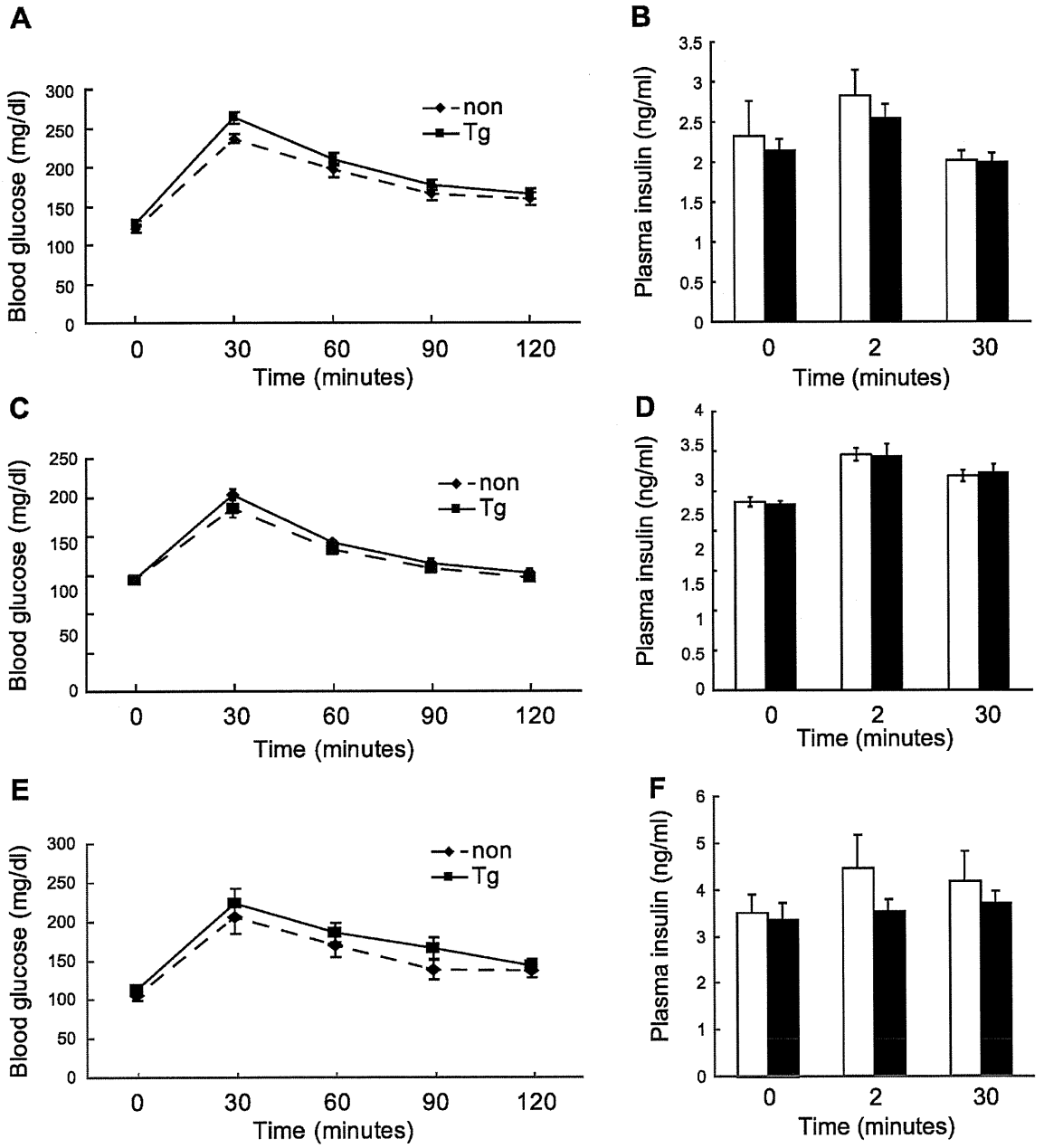

Fig. 5. Glucose metabolism in RIP-GG Tg mice. *A*, *C*, and *E*: glucose tolerance tests in 10-wk-old male (*A*), 11-wk-old female (*C*), or 83-wk-old male (*E*) Tg on MCTD (■) and non (♦); n = 7–10. *B*, *D*, and *F*: serum insulin levels at baseline and at 2 or 30 min after intravenous glucose injection in 15-wk-old male (*B*), 10-wk-old female (*D*), or 84-wk-old male (*F*) Tg fed MCTD (black bars) and in non (open bars); n = 5–10.

Staining intensities for these four islet hormones within islets of RIP-GG Tg mice did not differ from those of nontransgenic littermates.

DISCUSSION

In previous studies, we developed transgenic mice in which mouse ghrelin cDNA is overexpressed in pancreatic β-cells under the control of the rat insulin II promoter to identify the effect of ghrelin on pancreatic islets (15). However, these Tg mice displayed elevated expression of desacyl ghrelin only within the pancreas. At that time, the mechanism by which ghrelin received an *n*-octanoyl modification was unknown. Recently, Yang et al. (29) identified GOAT as the enzyme mediating this modification. In this study, we developed a transgenic mouse in which ghrelin produced in the pancreas might be both overexpressed and modified, with the overexpression of both mouse ghrelin and GOAT cDNA in pancreatic β-cells under the control of the rat insulin II promoter.

To our surprise, whereas pancreatic desacyl ghrelin levels were elevated in RIP-GG Tg mice, pancreatic levels of (active, modified) ghrelin were unchanged on a SD. Ghrelin levels were elevated only when mice were fed a MCTD. Similar results were reported by Kirchner et al. (16), who created a transgenic mouse in which ghrelin and GOAT cDNA were overexpressed in the liver under the control of

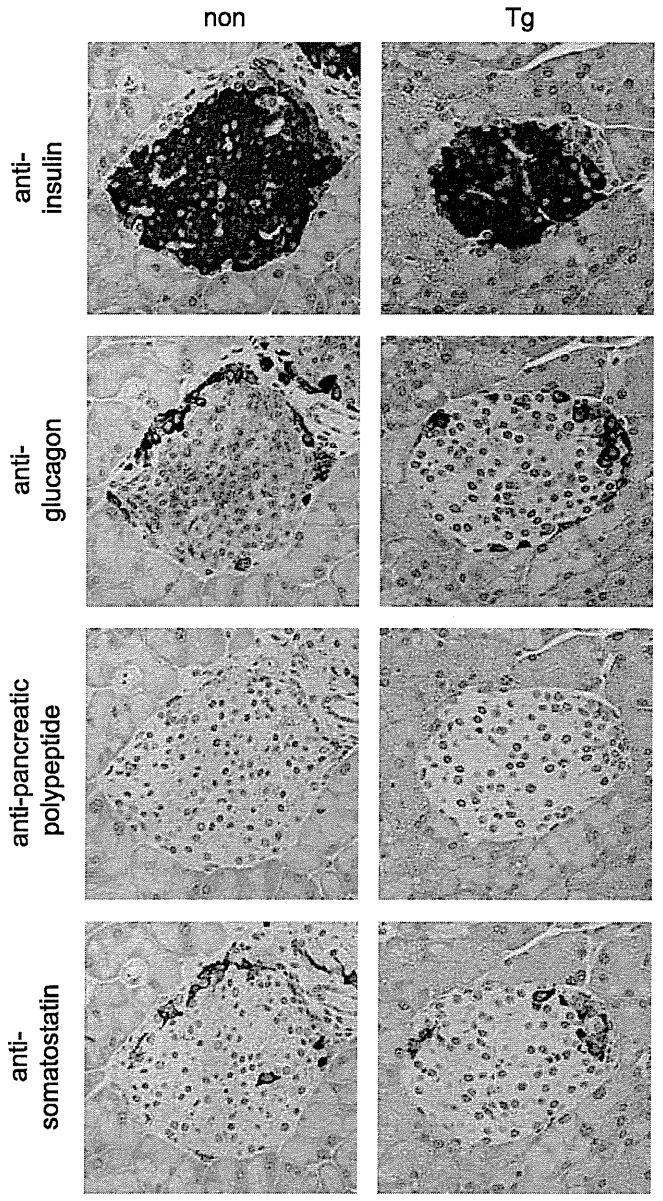

Fig. 6. Islet morphology in RIP-GG Tg mice. The pancreatic sections from RIP-GG Tg mice and non were stained with anti-insulin, anti-glucagon, anti-somatostatin, or anti-pancreatic polypeptide antibodies. Representative images are presented.

the apolipoprotein E promoter. These mice demonstrated elevated plasma ghrelin levels only when mice were fed a medium-chain fatty acid-rich diet. Considering that gastric ghrelin-producing cells can produce ghrelin regardless of diet, even in a fasting state, it is likely that these gastric cells possess a specific machinery to generate the octanoyl acid necessary for acylation, which is lacking from pancreatic β-cells or hepatocytes.

In previous studies, we demonstrated that the chronic elevation of plasma ghrelin levels at ~10-fold higher than the normal range suppresses insulin secretion and induces glucose intolerance in mice (13). In this study, RIP-GG Tg mice, which produce 16-fold higher ghrelin levels from the pancreas as normal mice, exhibited normal glucose tolerance and insulin secretion. The pancreatic ghrelin levels in RIP-GG Tg mice, although elevated, were still considerably lower than the gastric ghrelin level. We tried to compare the ghrelin levels in pancreatic vein with those in artery, as Dezaki et al. (7) did using rats, but it was difficult to determine the ghrelin levels in pancreatic veins of mice due to the small body size. We measured ghrelin levels in the portal vein instead, which were not elevated in RIP-GG Tg mice. We cannot determine the exact concentration of ghrelin in the microenvironment surrounding β-cells, but these levels still seem to be overpowered by the circulating ghrelin produced by the stomach. Although it is possible that additional overproducing of ghrelin in islets could eventually suppress insulin secretion, further enhancement of ghrelin expression by islets would not be in the realm of physiological relevance. In vitro, intraislet ghrelin may suppress insulin secretion in a paracrine (or autocrine) manner where the effect of circulating ghrelin is eliminated (6). However, this study indicates that intraislet ghrelin does not play a major role in controlling insulin secretion in vivo, where high levels of circulating ghrelin are generated by the stomach.

One drawback of this study is that elevated pancreatic ghrelin levels in RIP-GG Tg mice could not be obtained without feeding mice a MCTD. The MCTD consists of medium-chain fatty acids (C6–C10) that can enter mitochondria without the carnitine shuttle. Medium-chain triglycerides generally have favorable effects on obesity or diabetes (19), suppressing fat accumulation and improving insulin sensitivity. We cannot exclude the possibility that a MCTD may have interfered with the effects of ghrelin within islets. In addition, ghrelin and GOAT mRNA levels were increased not only in the islet but also in the hypothalamus of RIP-GG Tg mice. There is a possibility that the overexpressed ghrelin in the hypothalamus may have influenced the effects of overexpressed ghrelin in the islet.

In summary, we have developed RIP-GG Tg mice, in which intraislet ghrelin levels were elevated to ~16 times the control levels when mice were fed a MCTD. The glucose tolerance and insulin secretion of RIP-GG Tg mice were unchanged, indicating that intraislet ghrelin does not play a major role in regulating insulin secretion in vivo.

ACKNOWLEDGMENTS

We thank Chieko Ishimoto and Chinami Shiraiwa for their excellent technical assistance.

GRANTS

This study was supported by funds from the Ministry of Education, Culture, Sports, Science, and Technology of Japan and the Ministry of Health, Labour, and Welfare of Japan.

DISCLOSURES

The authors have nothing to declare.

AUTHOR CONTRIBUTIONS

M.B., H.I., and H.H. performed the experiments; M.B. and H.I. analyzed the data; M.B., H.I., H.A., H.H., G.Y., K.H., S.A., K.N., K.K., and T.A. interpreted the results of the experiments; M.B. and H.I. prepared the figures; M.B., H.I., and T.A. drafted the manuscript; M.B., H.I., H.A., K.H., S.A., K.N., K.K., and T.A. edited and revised the manuscript; M.B., H.I., K.N., K.K., and T.A. approved the final version of the manuscript; H.I., K.H., K.N., K.K., and T.A. did the conception and design of the research.

REFERENCES

1. **Adeghate E, Ponery AS.** Ghrelin stimulates insulin secretion from the pancreas of normal and diabetic rats. *J Neuroendocrinol* 14: 555–560, 2002.
2. **Bewick GA, Kent A, Campbell D, Patterson M, Ghatei MA, Bloom SR, Gardiner JV.** Mice with hyperghrelinemia are hyperphagic and glucose intolerant and have reduced leptin sensitivity. *Diabetes* 58: 840–846, 2009.
3. **Broglio F, Arvat E, Benso A, Gottero C, Muccioli G, Papotti M, van der Lely AJ, Deghenghi R, Ghigo E.** Ghrelin, a natural GH secretagogue produced by the stomach, induces hyperglycemia and reduces insulin secretion in humans. *J Clin Endocrinol Metab* 86: 5083–5086, 2001.
4. **Colombo M, Gregersen S, Xiao J, Hermansen K.** Effects of ghrelin and other neuropeptides (CART, MCH, orexin A and B, and GLP-1) on the release of insulin from isolated rat islets. *Pancreas* 27: 161–166, 2003.
5. **Date Y, Nakazato M, Hashiguchi S, Dezaki K, Mondal MS, Hosoda H, Kojima M, Kangawa K, Arima T, Matsuo H, Yada T, Matsukura S.** Ghrelin is present in pancreatic alpha-cells of humans and rats and stimulates insulin secretion. *Diabetes* 51: 124–129, 2002.
6. **Dezaki K, Hosoda H, Kakei M, Hashiguchi S, Watanabe M, Kangawa K, Yada T.** Endogenous ghrelin in pancreatic islets restricts insulin release by attenuating Ca2+ signaling in beta-cells: implication in the glycemic control in rodents. *Diabetes* 53: 3142–3151, 2004.
7. **Dezaki K, Sone H, Koizumi M, Nakata M, Kakei M, Nagai H, Hosoda H, Kangawa K, Yada T.** Blockade of pancreatic islet-derived ghrelin enhances insulin secretion to prevent high-fat diet-induced glucose intolerance. *Diabetes* 55: 3486–3493, 2006.
8. **Dornonville de la Cour C, Björkqvist M, Sandvik AK, Bakke I, Zhao CM, Chen D, Håkanson R.** A-like cells in the rat stomach contain ghrelin and do not operate under gastrin control. *Regul Pept* 99: 141–150, 2001.
9. **Egido EM, Rodriguez-Gallardo J, Silvestre RA, Marco J.** Inhibitory effect of ghrelin on insulin and pancreatic somatostatin secretion. *Eur J Endocrinol* 146: 241–244, 2002.
10. **Gnanapavan S, Kola B, Bustin SA, Morris DG, McGee P, Fairclough P, Bhattacharya S, Carpenter R, Grossman AB, Korbonits M.** The tissue distribution of the mRNA of ghrelin and subtypes of its receptor, GHS-R, in humans. *J Clin Endocrinol Metab* 87: 2988, 2002.
11. **Granata R, Settanni F, Biancone L, Trovato L, Nano R, Bertuzzi F, Destefanis S, Annunziata M, Martinetti M, Catapano F, Ghè C, Isgaard J, Papotti M, Ghigo E, Muccioli G.** Acylated and unacylated ghrelin promote proliferation and inhibit apoptosis of pancreatic beta-cells and human islets: involvement of 3′,5′-cyclic adenosine monophosphate/protein kinase A, extracellular signal-regulated kinase 1/2, and phosphatidyl inositol 3-Kinase/Akt signaling. *Endocrinology* 148: 512–529, 2007.
12. **Hosoda H, Kojima M, Matsuo H, Kangawa K.** Ghrelin and des-acyl ghrelin: two major forms of rat ghrelin peptide in gastrointestinal tissue. *Biochem Biophys Res Commun* 279: 909–913, 2000.
13. **Iwakura H, Ariyasu H, Li Y, Kanamoto N, Bando M, Yamada G, Hosoda H, Hosoda K, Shimatsu A, Nakao K, Kangawa K, Akamizu T.** A mouse model of ghrelinoma exhibited activated growth hormone-insulin-like growth factor I axis and glucose intolerance. *Am J Physiol Endocrinol Metab* 297: E802–E811, 2009.
14. **Iwakura H, Hosoda K, Doi R, Komoto I, Nishimura H, Son C, Fujikura J, Tomita T, Takaya K, Ogawa Y, Hayashi T, Inoue G, Akamizu T, Hosoda H, Kojima M, Kangawa K, Imamura M, Nakao K.** Ghrelin expression in islet cell tumors: augmented expression of ghrelin in a case of glucagonoma with multiple endocrine neoplasm type I. *J Clin Endocrinol Metab* 87: 4885–4888, 2002.
15. **Iwakura H, Hosoda K, Son C, Fujikura J, Tomita T, Noguchi M, Ariyasu H, Takaya K, Masuzaki H, Ogawa Y, Hayashi T, Inoue G, Akamizu T, Hosoda H, Kojima M, Itoh H, Toyokuni S, Kangawa K, Nakao K.** Analysis of rat insulin II promoter-ghrelin transgenic mice and rat glucagon promoter-ghrelin transgenic mice. *J Biol Chem* 280: 15247–15256, 2005.
16. **Kirchner H, Gutierrez JA, Solenberg PJ, Pfluger PT, Czyzyk TA, Willency JA, Schürmann A, Joost HG, Jandacek RJ, Hale JE, Heiman ML, Tschöp MH.** GOAT links dietary lipids with the endocrine control of energy balance. *Nat Med* 15: 741–745, 2009.
17. **Kojima M, Hosoda H, Date Y, Nakazato M, Matsuo H, Kangawa K.** Ghrelin is a growth-hormone-releasing acylated peptide from stomach. *Nature* 402: 656–660, 1999.
18. **Lee HM, Wang G, Englander EW, Kojima M, Greeley GH Jr.** Ghrelin, a new gastrointestinal endocrine peptide that stimulates insulin secretion: enteric distribution, ontogeny, influence of endocrine, and dietary manipulations. *Endocrinology* 143: 185–190, 2002.
19. **Nagao K, Yanagita T.** Medium-chain fatty acids: functional lipids for the prevention and treatment of the metabolic syndrome. *Pharmacol Res* 61: 208–212, 2010.
20. **Prado CL, Pugh-Bernard AE, Elghazi L, Sosa-Pineda B, Sussel L.** Ghrelin cells replace insulin-producing beta cells in two mouse models of pancreas development. *Proc Natl Acad Sci USA* 101: 2924–2929, 2004.
21. **Reed JA, Benoit SC, Pfluger PT, Tschöp MH, D'Alessio DA, Seeley RJ.** Mice with chronically increased circulating ghrelin develop age-related glucose intolerance. *Am J Physiol Endocrinol Metab* 294: E752–E760, 2008.
22. **Reimer MK, Pacini G, Ahren B.** Dose-dependent inhibition by ghrelin of insulin secretion in the mouse. *Endocrinology* 144: 916–921, 2003.
23. **Sun Y, Asnicar M, Saha PK, Chan L, Smith RG.** Ablation of ghrelin improves the diabetic but not obese phenotype of ob/ob mice. *Cell Metab* 3: 379–386, 2006.
24. **Takahashi H, Kurose Y, Kobayashi S, Sugino T, Kojima M, Kangawa K, Hasegawa Y, Terashima Y.** Ghrelin enhances glucose-induced insulin secretion in scheduled meal-fed sheep. *J Endocrinol* 189: 67–75, 2006.
25. **Tong J, Prigeon RL, Davis HW, Bidlingmaier M, Kahn SE, Cummings DE, Tschöp MH, D'Alessio D.** Ghrelin suppresses glucose-stimulated insulin secretion and deteriorates glucose tolerance in healthy humans. *Diabetes* 59: 2145–2151, 2010.
26. **Volante M, Allia E, Gugliotta P, Funaro A, Broglio F, Deghenghi R, Muccioli G, Ghigo E, Papotti M.** Expression of ghrelin and of the GH secretagogue receptor by pancreatic islet cells and related endocrine tumors. *J Clin Endocrinol Metab* 87: 1300–1308, 2002.
27. **Wierup N, Svensson H, Mulder H, Sundler F.** The ghrelin cell: a novel developmentally regulated islet cell in the human pancreas. *Regul Pept* 107: 63–69, 2002.
28. **Wierup N, Yang S, McEvilly RJ, Mulder H, Sundler F.** Ghrelin is expressed in a novel endocrine cell type in developing rat islets and inhibits insulin secretion from INS-1 (832/13) cells. *J Histochem Cytochem* 52: 301–310, 2004.
29. **Yang J, Brown MS, Liang G, Grishin NV, Goldstein JL.** Identification of the acyltransferase that octanoylates ghrelin, an appetite-stimulating peptide hormone. *Cell* 132: 387–396, 2008.

Diabetologia (2012) 55:1689–1698
DOI 10.1007/s00125-012-2508-2

ARTICLE

Induced pluripotent stem cells generated from diabetic patients with mitochondrial DNA A3243G mutation

J. Fujikura · K. Nakao · M. Sone · M. Noguchi · E. Mori · M. Naito · D. Taura · M. Harada-Shiba · I. Kishimoto · A. Watanabe · I. Asaka · K. Hosoda · K. Nakao

Received: 4 December 2011 / Accepted: 30 January 2012 / Published online: 7 March 2012

Abstract
Aims/hypothesis The aim of this study was to generate induced pluripotent stem (iPS) cells from patients with mitochondrial DNA (mtDNA) mutation.
Methods Skin biopsies were obtained from two diabetic patients with mtDNA A3243G mutation. The fibroblasts thus obtained were infected with retroviruses encoding *OCT4* (also known as *POU5F1*), *SOX2*, *c-MYC* (also known as *MYC*) and *KLF4*. The stem cell characteristics were investigated and the mtDNA mutation frequencies evaluated by Invader assay.
Results From the two diabetic patients we isolated four and ten putative mitochondrial disease-specific iPS (Mt-iPS) clones, respectively. Mt-iPS cells were cytogenetically normal and positive for alkaline phosphatase activity, with the pluripotent stem cell markers being detectable by immunocytochemistry. The cytosine guanine dinucleotide islands in the promoter regions of *OCT4* and *NANOG* were highly unmethylated, indicating epigenetic reprogramming to pluripotency. Mt-iPS clones were able to differentiate into derivatives of all three germ layers in vitro and in vivo. The Mt-iPS cells exhibited a bimodal degree of mutation heteroplasmy. The mutation frequencies decreased to an undetectable level in six of 14 clones, while the others showed several-fold increases in mutation frequencies (51–87%) compared with those in the original fibroblasts (18–24%). During serial cell culture passage and after differentiation, no recurrence of the mutation or no significant changes in the levels of heteroplasmy were seen.
Conclusions/interpretation iPS cells were successfully generated from patients with the mtDNA A3243G mutation. Mutation-rich, stable Mt-iPS cells may be a suitable source of cells for human mitochondrial disease modelling in vitro. Mutation-free iPS cells could provide an unlimited, disease-free supply of cells for autologous transplantation therapy.

Keywords Gene therapy · Monogenic forms of diabetes · Stem cells

Abbreviations

EB	Embryoid body
ES	Embryonic stem
FOXA2	Forkhead box A2
iPS	Induced pluripotent stem
MELAS	Mitochondrial encephalopathy lactic acidosis and stroke-like episodes

Junji Fujikura and Kazuhiro Nakao contributed equally to this study.

Electronic supplementary material The online version of this article (doi:10.1007/s00125-012-2508-2) contains peer-reviewed but unedited supplementary material, which is available to authorised users.

J. Fujikura (✉) · K. Nakao · M. Sone · M. Noguchi · E. Mori · M. Naito · D. Taura · K. Nakao (✉)
Department of Medicine and Clinical Science,
Kyoto University Graduate School of Medicine,
54 Shogoin Kawahara-cho, Sakyo-ku,
Kyoto 606-8507, Japan
e-mail: j-fuji@sannet.ne.jp
e-mail: nakao@kuhp.kyoto-u.ac.jp

M. Harada-Shiba · I. Kishimoto
Department of Endocrinology and Metabolism,
National Cerebral and Cardiovascular Center,
Osaka, Japan

A. Watanabe · I. Asaka
Center for iPS Cell Research and Application (CiRA),
Institute for Integrated Cell-Material Sciences,
Kyoto, Japan

K. Hosoda
Department of Human Health Science,
Kyoto University Graduate School of Medicine,
Kyoto, Japan

MERRF	Myoclonic epilepsy and ragged-red fibres
Mt1	Mt-iPS patient 1
Mt2	Mt-iPS patient 2
mtDNA	Mitochondrial DNA
Mt-iPS	Mitochondrial disease-specific iPS
NANOG	Nanog homeobox
SCID	Severe combined immunodeficient
α-SMA	α-Smooth muscle actin
SOX	SRY (sex determining region Y)-box
SSEA	Stage-specific embryonic antigen
TRA	Tumour rejection antigen

Introduction

Mitochondrial DNA (mtDNA) is present inside mitochondria and codes for components essential for cellular energy production [1]. mtDNA mutations cause degenerative human diseases. The tRNA (Leu) A3243G mutation is one of the most frequently observed mutations of mtDNA and is associated with a wide range of clinical phenotypes, including diabetes mellitus, hearing loss, cardiomyopathy, and mitochondrial encephalopathy, lactic acidosis and stroke-like episodes (MELAS) [2].

The mode of inheritance of mitochondrial diseases is maternal, but the penetrance of the disease is variable [3]. It is not possible to predict the phenotypes of children on the basis of the mother's genotypes and phenotypes, because the segregation of mtDNA tends to follow a pattern of random genetic drift [3]. This is the case for somatic cells and germ cells: it is not possible to predict to which cell types mutant mtDNA will dominantly migrate during development. To date, there is no specific therapy or cure for mitochondrial diseases, only supportive treatment. Efforts to understand the underlying genetics and pathophysiology of mitochondrial diseases have been hampered by the lack of a disease model.

Recently, human induced pluripotent stem (iPS) cells were successfully induced from adult skin fibroblasts [4]. iPS cells are biologically indistinguishable from embryonic stem (ES) cells. Human iPS cells, like ES cells, can differentiate into a variety of cell types and may therefore be another cell source for regenerative medicine. We have previously reported on angiogenic and adipogenic differentiation of human iPS and ES cells [5, 6]. More recently, disease-specific iPS cells have been generated from fibroblasts obtained from patients with various diseases [7–14], although not with mitochondrial diseases. The purpose of the present study was to derive iPS cells from patients with mitochondrial diseases and to evaluate the mtDNA of these cells.

Methods

Generation of mitochondrial disease-specific iPS cells Skin biopsies were undertaken after informed consent under protocols approved by the Ethics Committee of Kyoto University. Skin samples (4 mm) were minced with scalpels into smaller pieces and tissue fragments were placed into a tissue culture dish under a sterile coverslip. Medium (DMEM supplemented with 10% FBS (wt/vol.) and penicillin/streptomycin; Invitrogen, Carlsbad, CA, USA) was added to completely immerse the coverslip, and dishes were incubated at 37°C in a humidified incubator (5% CO_2). Fibroblasts grew out of the tissue fragments and when sufficiently numerous, cells were trypsinised and expanded. Cell cloning by limiting dilution in 96-well microtitre plates was employed at passage five.

The generation of iPS cells was performed according to the protocol of Ohnuki et al. [15]. In brief, the mouse ecotropic retrovirus receptor *Slc7a1* gene (Addgene, www.addgene.org/) was introduced to patient-derived fibroblasts at around passage number four by infection with lentivirus for 24 h. Retrovirus production was carried out for 24 h in Plat-E packaging cells via transfection with pMXs-hOCT4, pMXs-hSOX2, pMXs-hKLF4, pMXs-hc-MYC (Addgene) [16]. Fibroblasts expressing the mouse *Slc7a1* gene were then infected with retroviral cocktail. Next day, the medium was replaced with DMEM supplemented with 10% FBS (wt/vol.). After 6 days of transduction, infected fibroblasts were re-seeded on mouse fibroblast STO cell line feeder cells [17]. The medium was replaced the following day with human ES cell medium (ReproCELL; ReproCELL, Yokohama, Japan) supplemented with 4 ng/ml basic fibroblast growth factor (Wako, Osaka, Japan) and changed every 2 days. Starting 4 weeks after infection, colonies were picked on the basis of their morphological resemblance to human ES cell colonies and transferred on to mouse fibroblast STO cell line feeder cells in six-well plates; we defined this stage as passage one. Cultures were maintained on mouse fibroblast STO cell line feeders and passaged every 5 to 7 days enzymatically using 0.25% (wt/vol.) trypsin with 0.1 mg/ml collagenase type IV. Two human ES cell lines (H9 and KhES-1) and two human iPS cell lines (B7 and G1) were cultured and collected for genomic DNA analysis [4, 18–20].

Quantitative assessment of mtDNA mutation frequencies by Invader assay The primary probes and the invader oligo used to detect A3243G heteroplasmy were as follows: primary probe for 3243A: 5′-CGCGCCGAGGAGCCCGGTAATCGC<amino>–3′; primary probe for 3243G: 5′-ACGGACGCGGAGGGCCCGGTAATCG<amino>–3′; common Invader oligo: 5′-CCCACCCAAGAACAGGGTTTGTTAAGATGGCAGT-3′. The first 10 and 12 positions in the primary

probes represent the 5′ flap of Invader reaction. The cleavage enzyme, fluorescence resonance energy transfer probe, signal probe and Invader oligo were added to the microplates, including diluted plasmids that included the primary probe/Invader oligo binding region, after which the Invader assay was carried out as previously described [21]. The plates were incubated at 63°C in the fluorescence microplate reader (FluoDia-T70; Otsuka Electronics, Osaka, Japan). Fluorescence values for carboxyfluorescein (3243A; wavelength/bandwidth: excitation 485/20 nm; emission 530/25 nm) and Redmond red (3243G; excitation 560/20 nm; emission 620/40 nm) were measured every 2 min for a period of 4 h. To detect A3243G heteroplasmy, we calculated the copy number of 3243A and 3243G with a standard curve using quantitative Invader assay as described [21, 22]. The A3243G ratio was based on the ratio of the all-copy (3243A and 3243G) to the 3243A copy. In this assay, the lowest detection limit of the mutation frequency is 2%. The mtDNA A3243G mutation was also analysed by PCR-RFLP or fluorescent correlation spectroscopy [23–25].

Immunocytochemistry and alkaline phosphatase staining Immunocytochemistry was carried out as previously described [26]. The anti-human primary antibodies included: stage-specific embryonic antigen (SSEA)-1, SSEA-3, SSEA-4, tumour rejection antigen (TRA)-1-60, TRA-1-81 (all from Stemgent, San Diego, CA, USA), Nanog homeobox (NANOG) (R&D Systems, Minneapolis, MN, USA), β3 tubulin (Millipore, Temecula, CA, USA), α-smooth muscle actin (α-SMA) (Sigma-Aldrich, Saint Louis, MO, USA), forkhead box A2 (FOXA2) (Cell Signaling Technology, Danvers, MA, USA) and SRY (sex determining region Y)-box (SOX)17 (R&D Systems).

For immunofluorescence, Alexa Fluor 488 goat anti-mouse IgM, Alexa Fluor 488 goat anti-rat IgM, Alexa Fluor 488 goat anti-mouse IgG, Alexa Fluor 546 rabbit anti-goat IgG and Alexa Fluor 546 goat anti-mouse IgG (all from Molecular Probes, Eugene, OR, USA) served as the secondary antibody. Alkaline phosphatase activity was detected using a kit (Alkaline Phosphatase Staining Kit; Stemgent). Images were captured using a microscope (Olympus IX81; Olympus, Tokyo, Japan).

Karyotype analysis Standard G-banding chromosome analysis was performed in the Nihon Gene Research Laboratories (Sendai, Japan) or Chromosome Science Lab (Sapporo, Japan). Selected iPS clones (mitochondrial disease-specific [Mt-iPS] patient 1 [Mt1] clone 1 [Mt1-1], Mt1-4, Mt-iPS patient 2 [Mt2] clone 3 [Mt2-3] and Mt2-6) were analysed at passages 18 to 27.

Bisulphite genomic sequencing Genomic DNA (1 μg) from Mt-iPS cells was processed for bisulphite modification using a kit (EZ DNA Methylation Gold; Zymoresearch, Irvine, CA, USA). The cytosine guanine dinucleotide-rich promoter regions of *OCT4* (also known as *POU5F1*) and *NANOG* were selected to be amplified by PCR with ExTaq Hot start (Takara, Kyoto, Japan). The PCR products were subcloned into pCR4 vector (Life Technologies, Carlsbad, CA, USA). Ten clones of each sample were verified by sequencing with Sp6 universal primer.

Short tandem repeat analysis The genomic DNA was used for PCR with Cell ID System (Promega, Madison, WI, USA) and analysed by genetic analyser (ABI PRISM 3100) and GeneMapper version 3.5 (both from Applied Biosystems, Foster City, CA, USA).

In vitro differentiation by embryoid body formation and M15 co-culture Spontaneous differentiation through embryoid body (EB) formation was initiated by dissociation of Mt-iPS cells using collagenase/trypsin treatment, with subsequent transfer to low-attachment multi-well plates in ReproCELL medium. The medium was changed every second day. After 8 days of floating culture, tentative iPS (Mt-iPS) clones formed EBs and were transferred to 0.1% (wt/vol.) gelatin-coated plates to induce further differentiation for 8 days. Differentiated markers such as β3-tubulin, α-SMA and FOXA2 were analysed by immunocytochemistry.

Endodermal differentiation was performed according to Shiraki et al. [27]. In brief, dissociated Mt-iPS cells were inoculated on to multi-well plates containing a feeder layer of mitomycin C-treated M15 cells [28] in medium (DMEM supplemented with 10% FBS (wt/vol.) and penicillin/streptomycin; Invitrogen). The medium was changed every second day. After 2 weeks of culture, genomic DNA was extracted for the Invader assay. Endodermal differentiation was confirmed by immunocytochemistry with antibodies against FOXA2 and SOX17.

Teratoma formation Approximately 5×10^5 iPS cells were collected by collagenase/trypsin treatment and injected into the testicles of 7- to 12-week-old severe combined immunodeficient (SCID) mice. Teratomas were collected 9 to 12 weeks after injection and fixed with 10% (wt/vol.) buffered neutral formalin. Paraffin-embedded tissues were sectioned and stained with haematoxylin and eosin. Animal studies were conducted in accordance with our institutional guidelines and approved by Kyoto University Animal Care Committee.

Determination of mtDNA content Genomic DNA was extracted from blood, fibroblasts and Mt-iPS cells using a kit (DNeasy Tissue Kit; Qiagen, Valencia, CA, USA) or a standard established protocol [29]. The extracted DNA samples were stored at 4°C until assay. The relative mtDNA

copy numbers were measured by real-time PCR and corrected by measurement of the nuclear DNA [30]. The primers for mitochondrial *ND5* gene were 5′-AGGCGCTATCAC CACTCTGTTCG-3′ and 5′-AACCTGTGAGGAAAGG TATTCCTG-3′. The primers for nuclear *CF* (also known as *CFTR*) gene were 5′-AGCAGAGTACCTGAAACAGGAA-3′ and 5′-AGCTTACCCATAGAGGAAACATAA-3′. The PCR was performed using StepOnePlus Real-Time PCR (Applied Biosystems) and a quantitative PCR mix kit (Thunderbird SYBR qPCR Mix; Toyobo, Osaka, Japan). DNA (80 ng) was mixed with 10 μl SYBR qPCR containing 6 pmol of forward and reverse primers, and with ROX reference dye in a final volume of 20 μl. The PCR conditions were 1 min at 95°C, followed by 40 cycles of denaturation at 95°C for 15 s and of annealing and primer extension at 60°C for 60 s. Standard curves were generated using serial dilutions of plasmid DNA containing the PCR amplicons cloned into pGEM-T Easy (Promega). The threshold cycle number values of *ND5* and *CF* were determined in two DNA duplicate samples. The amplified products were denatured and re-annealed at different temperature points to detect their specific melting temperature.

Sample mtDNA content (mtDNA copies per cell) were calculated using the formula (*ND5* gene copies/*CF* gene copies)×2=mtDNA copies per cell.

Results

Generation of iPS cells from diabetic patients with the mtDNA A3243G mutation Skin biopsies were obtained from two Japanese patients who had diabetes mellitus, came from different families and carried the mtDNA A3243G mutation. Patient 1 (Mt1) was a 38-year-old man and patient 2 (Mt2) was a 46-year-old woman. Their clinical data are given in Table 1. Mt1 presented at 31 years of age with thirst, polydipsia, polyuria, tiredness and loss of body weight. His blood glucose concentration was 38.4 mmol/l and his HbA_{1c} level was 14.3% (132 mmol/mol). He responded well to insulin therapy as a way to control his diabetes. Mt2 was diagnosed with gestational diabetes at 24 years of age. She had a progressive hearing impairment. She had also suffered from epilepsy since the age of 27 years and had been treated with valproic acid. At 31 years of age she developed diabetic ketoacidosis and began insulin therapy. Both patients had a positive family history of maternal diabetes mellitus. The A3243G mtDNA mutation was identified by sequencing of PCR products amplified from peripheral blood genomic DNA from both patients (data not shown).

Two fibroblast lines (Mt1-fibro and Mt2-fibro) were obtained from skin biopsies of the two patients. Each fibroblast line was cultured and infected with a combination of retroviruses encoding the transcription factors octamer-binding protein 4 (OCT4), SOX2, proto-oncogene c-Myc (c-MYC) and Kruppel-like factor 4 (KLF4) [4]. Starting 4 weeks after infection, colonies were selected on the basis of their morphological resemblance to human ES cell colonies and expanded. We were able to isolate four (Mt1-1 to -4) and 10 (Mt2-1 to -10) putative iPS (Mt-iPS) clones from Mt1-fibro and Mt2-fibro lines, respectively.

mtDNA mutation frequencies in Mt-iPS cells The presence and levels of heteroplasmy in the patient-derived blood cells, fibroblasts (Mt1-fibro and Mt2-fibro) and putative iPS clones (Mt1-1 to -4 and Mt2-1 to -10) were evaluated (Fig. 1a). The Invader assay was used to quantify the heteroplasmy of the mtDNA A3243G mutation in Mt-iPS cells [31–33]. This method was originally developed to genotype single nucleotide polymorphisms and has been used to genotype mtDNA mutations and to quantify heteroplasmy. It is one of the most accurate ways of determining mtDNA heteroplasmy [34]. The passage numbers at which Mt-iPS cells were collected for the Invader assay were: Mt1-1 passage 12; Mt1-2 passage 16; Mt1-3 passage 17; Mt1-4 passage 14; Mt2-1 passage 9; Mt2-2 passage 8; Mt2-3 passage 10; Mt2-4 passage 9; Mt2-5 passage 10; Mt2-6 passage 10; Mt2-7 passage 7; Mt2-8 passage 7; Mt2-9 passage 9; Mt2-10 passage 11. Mutation frequencies in the peripheral blood cells from both patients were 24% (Mt1-blood 24%, Mt2-blood 24%). Skin-derived fibroblasts from both patients showed similar levels of mutation frequency compared with those of blood cells from the same patients (Mt1-fibro 18%, Mt2-fibro 24%). However, two of four Mt1-iPS clones (Mt1-1 and Mt1-2) and six of 10 Mt2-iPS clones (Mt2-1, Mt2-2, Mt2-3, Mt2-4, Mt2-7, Mt2-8) showed undetectable levels (<2%) of the A3243G mutation. Furthermore, marked elevations of the mutation frequencies compared with those of the original fibroblast lines were detected in other iPS lines (Mt1-3 51%, Mt1-4 87%, Mt2-5 83%, Mt2-6 69%, Mt2-9 79%, Mt2-10 74%). No significant associations were found between culture passage number of Mt-iPS cells and the mutation frequency. The absence and presence of the mutation were confirmed by PCR-RFLP and by gene analysis by fluorescence correlation spectroscopy [24, 25].

The mutation frequency of the fibroblasts was further assessed (Fig. 1b). The fibroblasts from patient 2 (Mt2-fibro) were cultured until passage 16 (for over 2 months). Fibroblast cell cloning by limiting dilution was performed from parental Mt2-fibro at passage five, and five fibroblast clones were obtained (Mt2-fibro-clone). Genomic DNA was extracted from Mt2-fibro at various passage points and from the five Mt2-fibro-clones at about 4 weeks after the cloning procedure. The mutation frequencies in Mt2-fibro gradually increased with increasing passage number of the cells

Table 1 Information on patient donors for generation of Mt1-iPS and Mt2-iPS cell lines

Patient	Age (years)	Sex	Family history	mtDNA mutation	Clinical abnormalities	BMI (kg/m^2)	Medication	HbA_{1c} (%)	
								%	mmol/mol
Mt1	38	Male	Mother: diabetes mellitus, cardiomyopathy	A3243G	Diabetes mellitus	18	Insulin 33 U/day	8.2	66.1
Mt2	46	Female	Mother: diabetes mellitus	A3243G	Diabetes mellitus, sensorineural hearing loss, epilepsy, cardiomyopathy	22	Insulin 30 U/day, valproic acid 600 mg/day	7.0	53.0

(Fig. 1b). All the Mt2-fibro-clones displayed high mutation frequencies and no mutation-free fibroblast clones were observed (Fig. 1b).

Characterisation of the Mt-iPS cells generated All the Mt-iPS clones showed typical human ES cell-like morphology (Fig. 2a, ESM Fig. 1). Mt-iPS cells were positive for alkaline phosphatase activity, and the pluripotent stem cell markers SSEA-3, SSEA-4, TRA-1-60, TRA-1-81 and NANOG were detected by immunocytochemical analyses in all 14 clones (Fig. 2a, ESM Fig. 1) [35]. Mt-iPS cells did not produce SSEA-1 except for a few cells at the edge of the colonies (Fig. 2a, ESM Fig. 1). The morphological and immunocytochemical characteristics of mutation-free and mutation-rich Mt-iPS cells were indistinguishable.

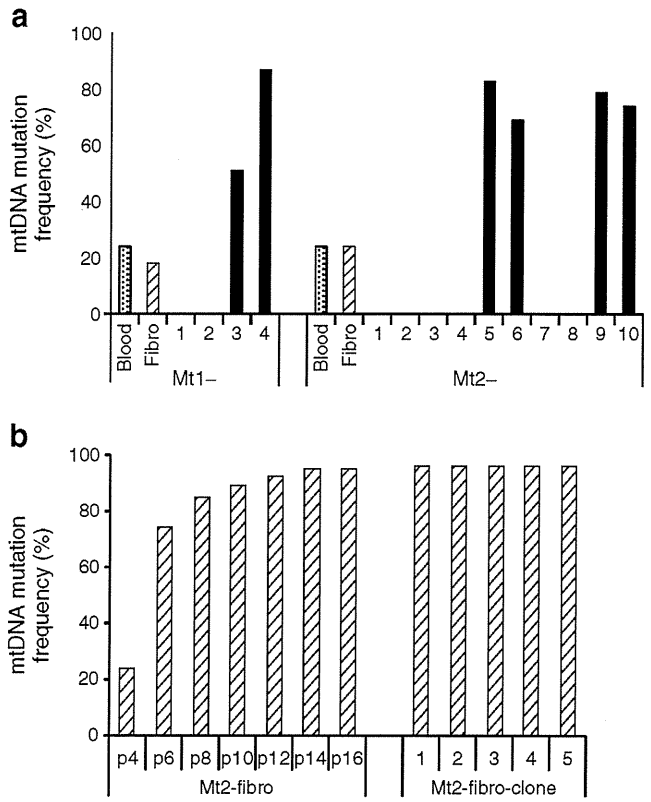

Fig. 1 mtDNA mutation frequencies in Mt-iPS cells. **a** mtDNA A3243G mutation frequencies in patient-derived blood cells (Mt1-blood, Mt2-blood), original fibroblasts (Mt1-fibro, Mt2-fibro) and Mt-iPS clones (Mt1-1 to Mt1-4, Mt2-1 to Mt2-10). Mt-iPS cells were collected at the following passage (p) numbers: Mt1-1 p12, Mt1-2 p16, Mt1-3 p17, Mt1-4 p14, Mt2-1 p9, Mt2-2 p8, Mt2-3 p10, Mt2-4 p9, Mt2-5 p10, Mt2-6 p10, Mt2-7 p7, Mt2-8 p7, Mt2-9 p9, Mt2-10 p11. **b** mtDNA A3243G mutation frequencies in Mt2-derived fibroblasts at various culture passage numbers and in isolated fibroblast clones. Limiting dilution was performed from the original fibroblasts (Mt2-fibro) at passage five and five fibroblast clones were obtained

To examine whether Mt-iPS clones are cytogenetically normal, karyotyping analyses were performed on selected Mt-iPS cells at passages 18 to 27. Both mutation-free (Mt1-1 and Mt2-3) and mutation-rich (Mt1-4 and Mt2-6) Mt-iPS clones from both patients maintained a normal karyotype (Fig. 2b, ESM Fig. 2).

Bisulphite genomic sequencing analyses evaluating the methylation statuses of cytosine guanine dinucleotides in the promoter regions of *OCT4* and *NANOG* revealed that they were highly unmethylated (Fig. 2c), indicating epigenetic reprogramming to pluripotency.

To confirm that the Mt-iPS clones were indeed derived from the patients, we performed DNA fingerprinting analyses with short tandem repeat markers. The short tandem repeat profiles of the Mt-iPS clones matched perfectly to those of their parental fibroblasts and of blood cells obtained from the patients (ESM Table 1). Thus, the Mt-iPS clones were indeed derived from the patients and were not a result of contamination.

Pluripotency of Mt-iPS cells by in vitro and in vivo differentiation Pluripotent cells are by definition capable of differentiating into cell types derived from each of the three embryonic germ layers [18]. To determine the differentiation ability of Mt-iPS cells in vitro, suspension culture for the formation of EBs was used [36]. After 8 days in suspension culture, iPS cells formed ball-shaped structures. These EBs were transferred to gelatin-coated plates and further cultured for another 8 days. Attached cells showed various types of morphologies, including those resembling neuronal cells, cobblestone-like cells and epithelial cells. Immunocytochemistry detected cells positive for β3-tubulin (a marker of ectoderm), α-SMA (a marker of mesoderm) or FOXA2 (a marker of endoderm) (Fig. 3a, ESM Fig. 3a). We

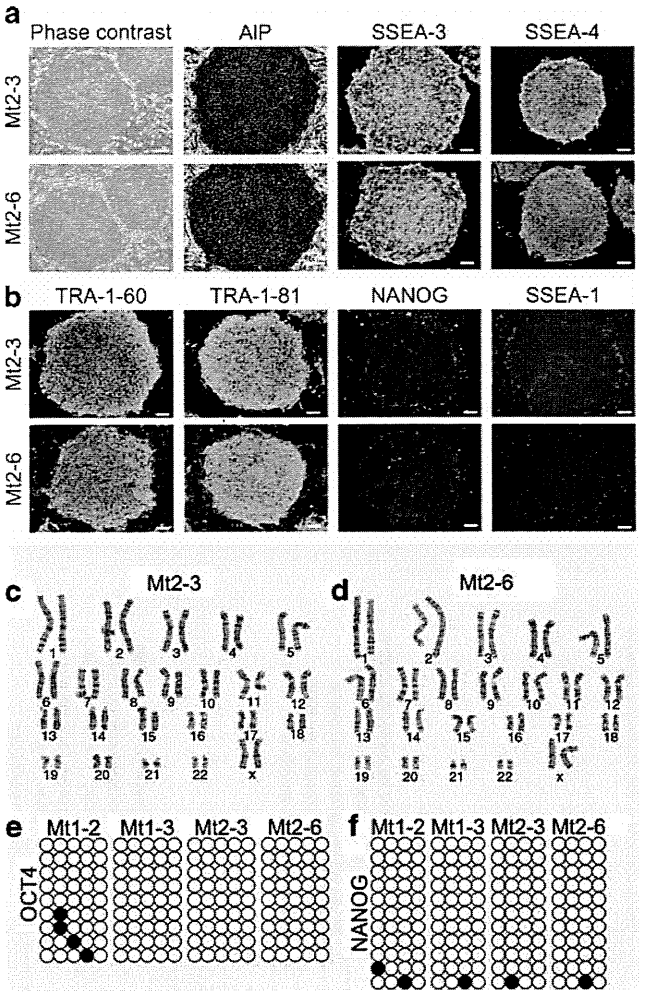

Fig. 2 Characterisation of generated Mt-iPS cells. **a, b** Colonies of Mt-iPS cells (Mt2-3 and Mt2-6) grown on mouse fibroblast STO cell line feeder cells showing human-ES-cell-like morphology. The detection of (**a**) alkaline phosphatase activity (AIP) and immunofluorescence analyses for the presence of the pluripotency markers SSEA-3, SSEA-4, and (**b**) TRA-1-60, TRA-1-81, NANOG and SSEA-1 are indicated. Scale bars 200 μm. **c** Karyotyping of Mt-iPS cells Mt2-3 and (**d**) Mt2-6 at passage 22. **e** Bisulphite genomic sequencing of the promoter regions of *OCT4* and (f) *NANOG*. White circles, unmethylated cytosine guanine dinucleotides; black circles, methylated cytosine guanine dinucleotides

found that all Mt-iPS clones were able to differentiate into three germ layers in vitro.

To determine pluripotency in vivo, we transplanted Mt-iPS cells into the testicles of SCID mice. At 9 weeks after injection, tumour formation was observed. Histological examination showed that the tumours contained various tissues, including pigmented epithelium (ectoderm), cartilage (mesoderm) and gut-like epithelial tissues (endoderm) (Fig. 3b, ESM Fig. 3b). Thus, Mt-iPS clones were able to spontaneously differentiate into derivatives of all three germ layers in vivo.

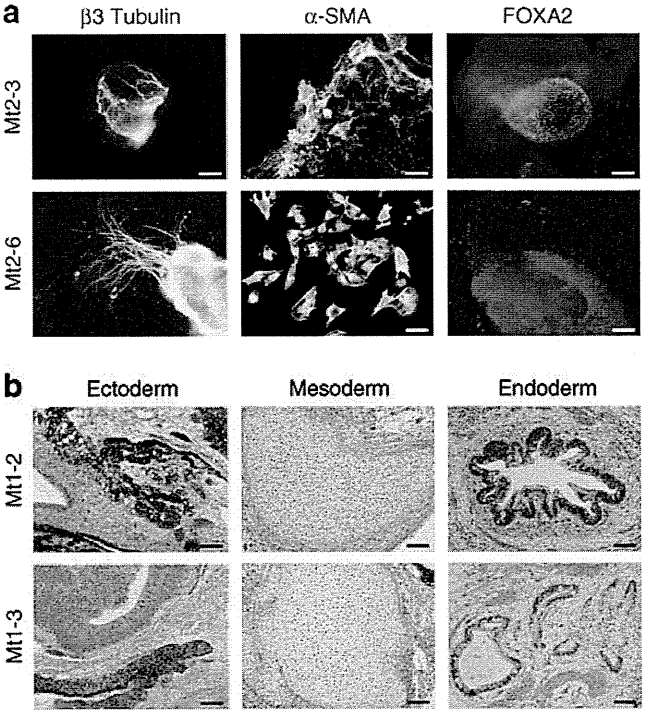

Fig. 3 Pluripotency of Mt-iPS cells by in vitro and in vivo differentiation. **a** In vitro differentiation of Mt-iPS cells (Mt2-3, Mt2-6) revealed their potential to generate cell derivatives of all three primary germ cell layers. Immunofluorescence analyses showed markers of neurectoderm (β3-tubulin), mesoderm (α-SMA) and endoderm (FOXA2). Images are overlays with a nuclear stain (DAPI). **b** Teratoma formation occurred after injection of Mt-iPS cells (Mt1-2, Mt1-3) into the testes of SCID mice (Japan Clea, Tokyo, Japan). Haematoxylin and eosin stainings of teratoma sections show derivatives of ectoderm (pigmented epithelial cells), mesoderm (cartilage) and endoderm (gut-like glandular structures). Scale bars, 100 μm

Influence of culture passage number and differentiation on mtDNA mutation frequencies in Mt-iPS cells We examined whether or not the mutation frequencies of Mt-iPS clones were fixed over the course of cell culturing and passage (Fig. 4a). Analysis of the same clones at various passage numbers revealed that no induction of mutation was observed in mutation-free Mt-iPS clones (Mt1-1, Mt1-2, Mt2-1, Mt2-3 and Mt2-8). Mutation frequencies of the mutation-rich Mt-iPS clones were relatively constant across passages (Mt1-3, Mt1-4, Mt2-6 and Mt2-10).

The influence of differentiation on mutation frequency was also examined in all the Mt-iPS clones (Fig. 4b). Analysis of the same clones in an undifferentiated state and after 16 days of differentiation as a result of spontaneous differentiation (EB formation) or directed differentiation into endodermal lineage (M15 co-culture) (ESM Fig. 4) showed no induction of mutation in mutation-free Mt-iPS clones (Mt1-1, Mt1-2, Mt2-1, Mt2-2, Mt2-3, Mt2-4, Mt2-7 and Mt2-8). The mutation frequencies of the mutation-rich Mt-iPS clones were relatively constant after differentiation (Mt1-3, Mt1-4, Mt2-5, Mt2-6, Mt2-9 and Mt2-10).

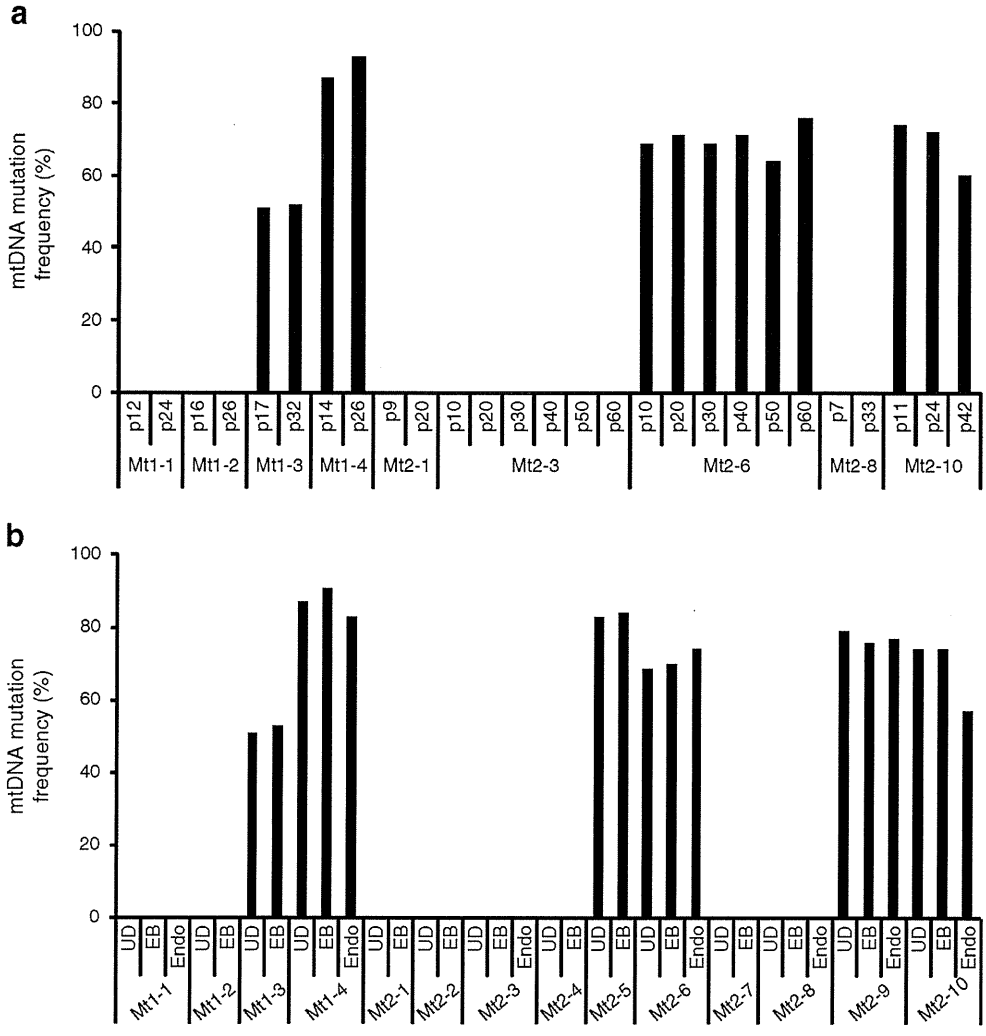

Fig. 4 Influence of culture passage number and differentiation on mtDNA mutation frequencies in Mt-iPS cells. **a** mtDNA A3243G mutation frequencies in undifferentiated Mt-iPS clones at various culture passage (p) numbers as indicated. **b** mtDNA A3243G mutation frequencies in undifferentiated (UD), differentiated EB (EB) and endodermal (Endo) states of Mt-iPS clones

mtDNA content in Mt-iPS cells The mtDNA content (mitochondrial genome copies per cell) in the blood cells, fibroblasts (Mt1-fibro and Mt2-fibro) and iPS clones was determined by quantitative genomic PCR (Fig. 5).

The skin fibroblast mtDNA content (Mt1-fibro 553 copies/cell; Mt2-fibro 4296 copies/cell) was higher than that in the peripheral blood (Mt1-blood 196 copies/cell; Mt2-blood 60 copies/cell). The mtDNA content of Mt-iPS cells at early passage was slightly lower than that in the original fibroblast cultures (Mt1-1 passage 12 454 copies/cell; Mt1-4 passage 14 151 copies/cell; Mt2-3 passage 10 2,100 copies/cell; Mt2-6 passage 10 1,709 copies/cell) (Fig. 5 and data not shown). The mtDNA content of Mt-iPS cells markedly decreased to levels close to those of human ES (H9 passage 87 79 copies/cell; KhES-1 passage 78 78 copies/cell) and iPS (B7 passsage 54 150 copies/cell; G1 passage 40 94 copies/cell) cells by passage number 20 (Mt1-4 passage 26 42 copies/cell; Mt2-3 passage 20 49 copies/cell; Mt2-6 passage 20 45 copies/cell) and was maintained thereafter (Mt2-3 passage 30 68 copies/cell; Mt2-6 passage 30 50 copies/cell). The mtDNA content of fibroblasts and iPS cells from Mt1 (Mt1-fibro, Mt1-1 passage 12 and Mt1-4passage 14) were lower than those from Mt2 (Mt2-fibro, Mt2-3

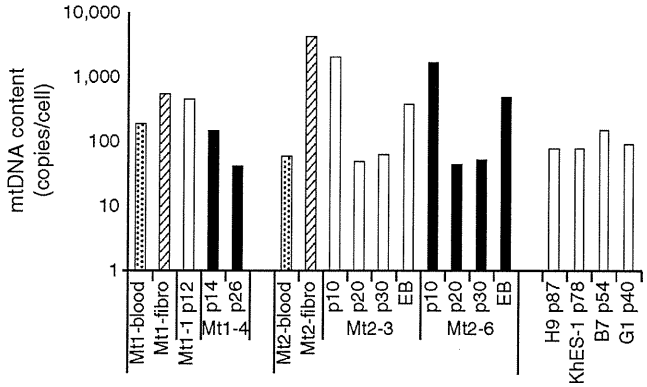

Fig. 5 mtDNA content in Mt-iPS cells. mtDNA content (copies/cell) in blood cells, fibroblasts, mutation-free iPS clones (Mt1-1, Mt2-3 white bars) and mutation-rich iPS clones (black bars). mtDNA from two human ES cell lines (H9 and KhES1) and two human iPS cell lines (B7 and G1) are also shown. p, passage. Mt-iPS cells at around p30 were used for EB formation and assayed for mtDNA contents (Mt2-3 EB, Mt2-6 EB)

passage 10 and Mt2-6 passage 10), although the content of each Mt-iPS clone was variable (data not shown).

The mtDNA copy number increased seven- to tenfold after EB differentiation (Mt2-3 passage 24-derived EB 384 copies/cell; Mt2-6 passage 24-derived EB 484 copies/cell). Major differences in mtDNA content were not found between mutation-free and mutation-rich iPS cells (Fig. 5 and data not shown).

Discussion

In the present study, we established human iPS cell lines from male and female diabetic patients with the mtDNA A3243G mutation. These cells have the features of pluripotent human ES cells, including the ability to differentiate into cell types of all embryonic lineages.

A striking feature of Mt-iPS shown in the present study is their bimodal levels of heteroplasmy. The mtDNA mutation frequencies decreased to undetectable levels in about half of the clones, while the other half showed a large increase in the levels of mutation heteroplasmy compared with those in the patients' original fibroblasts. The mechanisms underlying this phenomenon remain unclear; however, several possibilities exist in terms of the timing of heteroplasmy segregation. One is that the heteroplasmy levels in Mt-iPS clones simply reflect those in the original single fibroblast from which the iPS clones were derived. This is based on the assumption that the population of fibroblasts is bimodal (mutation-rich and mutation-free) with regard to levels of heteroplasmy, but we were not able to isolate any mutation-free fibroblast clone and hence could find no evidence of extreme mosaicism in the original fibroblasts. The second possibility is that changes in the levels of heteroplasmy occur during serial in vitro culture of Mt-iPS cells. Previous reports have shown age-related directional selection for different mtDNA genotypes in mouse tissues [37]; however, this is unlikely in our study because passage number did not significantly affect the mutation frequencies of Mt-iPS cells. The third and most likely possibility is that changes in the levels of heteroplasmy occur during reprogramming of patients' fibroblasts to iPS cells. Substantial shifts in the levels of mitochondrial heteroplasmy have been demonstrated to occur between single mammalian generations, and neutral mitochondrial genotypes have also been demonstrated to segregate in different directions in offspring from the same female (rapid segregation of mitochondrial genotype) [38–40]. Random partitioning of organelles with few mtDNA molecules into germ cells could account for the small number of segregating units and lead to the rapid segregation of polymorphic mtDNA species in the progeny.

The A3243G transition in the tRNA *Leu* gene is one of the most frequent mitochondrial mutations [2]. The phenotypic expression of the mutation is variable and may be associated with maternally inherited diabetes mellitus and deafness syndrome, myoclonic epilepsy and ragged-red fibres (MERRF) syndrome, MELAS/MERRF overlap syndrome, maternally inherited Leigh syndrome, and chronic external ophthalmoplegia or Kearns–Sayre syndrome. This heterogeneity is considered to result from the variable levels of heteroplasmy and the variability of tissue-specific thresholds for mitochondrial functions required for normal development and physiology [41]. There is currently no specific therapy or cure. The precise mechanisms for the generation of heteroplasmy and of mitochondrial dysfunction in these diseases remain to be elucidated. Mt-iPS cells offer several significant advantages for this research. The analysis of the process of iPS cell generation might help to clarify the mechanisms of mtDNA germ line segregation. This might further clarify the mode of inheritance of mitochondrial diseases, enabling pre-fertilisation diagnosis to be performed. We might also be able to study the process of mtDNA somatic segregation toward the target tissues involved in mitochondrial diseases after the induction of differentiation. Mutation-rich Mt-iPS cells should be useful as new types of disease models, in which the initiation and progression of the diseases can be studied. In this context, mutation-free Mt-iPS cells sharing the same nuclear genetic background could serve as ideal negative controls. These approaches could improve understanding of the cause of the disease and lead to the development of efficient preventive and therapeutic strategies. Ultimately, patient-specific and mutation-free Mt-iPS cells might be useful as a supplement or an alternative to disease-affected tissues in future. In this study, we generated Mt-iPS cells by retroviral transduction of *OCT4*, *SOX2*, *c-MYC* (also known as *MYC*) and *KLF4*; however, genomic integration of these transgenes increases the risk of tumorigenicity. By generating integration-free human iPS cells, we could safely transplant mtDNA-mutation-corrected cells without the use of potentially harmful DNA recombination technology [42]. mtDNA content is known to be a major determinant of mitochondrial gene expression [43]. Undifferentiated mouse and human ES cells have very low levels of mtDNA content (<100 copies/cell), but this rapidly increases up to several thousand-fold during differentiation [44–47]. However, it remains to be determined whether human iPS cells are able, like ES cells, to regulate their mtDNA copy number in their undifferentiated state. We have revealed here that the mtDNA content in Mt-iPS cells at early passage (around passage 10) is similar to that of the original fibroblasts, and that the mtDNA content at later passages (after passage 20) is similar to that of human ES cells. This indicates that the number of mitochondria gradually adapts to the new stem cell environment in iPS cells. Although compensatory amplification of the mitochondrial genome has been reported in patients with mtDNA mutations, the mtDNA content is relatively constant among Mt-iPS

clones, despite a wide variation in heteroplasmy levels [48–50]. These results also indicate that the cell viability and stemness are unaffected at the low metabolic demand of undifferentiated iPS cells, irrespective of the presence or absence of the A3243G mutation.

In conclusion, we have generated mitochondrial Mt-iPS cells. About half of the clones had undetectable levels of the mutation. By overcoming the immunological and ethical problems associated with ES cells, these Mt-iPS cells could provide a powerful new tool with which to investigate organ involvement and pathogenic mechanisms, and also to screen for new drugs in specific diseases, as well as opening new avenues for autologous cell transplantation therapy.

Acknowledgements We thank K. Nakada and K. Kuwahara for helpful discussions.

Funding This work was supported in part by research grants from: the Leading Project of the Ministry of Education, Culture, Sports, Science and Technology of Japan; the Ministry of Health, Labour and Welfare of Japan; the Takeda Medical Research Foundation; the Smoking Research Foundation; Suzuken Memorial Foundation; Japan Foundation of Applied Enzymology; Novo Nordisk (Insulin Research Award); and Lilly Education and Research Grant Office.

Contribution statement JF, Kazuhiro Nakao, MS, KH and Kazuwa Nakao contributed to study concept and design. JF, Kazuhiro Nakao, MN, EM, MN, DT, MH-S, IK, AW, IA and Kazuwa Nakao contributed to analysis and interpretation of data. JF, Kazuhiro Nakao, MS, MN, EM, MN, DT, MH-S, IK, AW, IA, KH and Kazuwa Nakao contributed to drafting of the manuscript. JF, Kazuhiro Nakao and Kazuwa Nakao contributed to critical revision of the manuscript for intellectual content. All the authors gave approval of the final version to be published.

Duality of interest The authors declare that there is no duality of interest associated with this manuscript.

References

1. May-Panloup P, Chretien MF, Malthiery Y, Reynier P (2007) Mitochondrial DNA in the oocyte and the developing embryo. Curr Top Dev Biol 77:51–83
2. Finsterer J (2009) Manifestations of the mitochondrial A3243G mutation. Int J Cardiol 137:60–62
3. Shoubridge EA, Wai T (2007) Mitochondrial DNA and the mammalian oocyte. Curr Top Dev Biol 77:87–111
4. Takahashi K, Tanabe K, Ohnuki M et al (2007) Induction of pluripotent stem cells from adult human fibroblasts by defined factors. Cell 131:861–872
5. Sone M, Itoh H, Yamahara K et al (2007) Pathway for differentiation of human embryonic stem cells to vascular cell components and their potential for vascular regeneration. Arterioscler Thromb Vasc Biol 27:2127–2134
6. Taura D, Noguchi M, Sone M et al (2009) Adipogenic differentiation of human induced pluripotent stem cells: comparison with that of human embryonic stem cells. FEBS Lett 583:1029–1033
7. Dimos JT, Rodolfa KT, Niakan KK et al (2008) Induced pluripotent stem cells generated from patients with ALS can be differentiated into motor neurons. Science 321:1218–1221
8. Ebert AD, Yu J, Rose FF Jr et al (2009) Induced pluripotent stem cells from a spinal muscular atrophy patient. Nature 457:277–280
9. Park IH, Arora N, Huo H et al (2008) Disease-specific induced pluripotent stem cells. Cell 134:877–886
10. Soldner F, Hockemeyer D, Beard C et al (2009) Parkinson's disease patient-derived induced pluripotent stem cells free of viral reprogramming factors. Cell 136:964–977
11. Liu J, Verma PJ, Evans-Galea MV et al (2011) Generation of induced pluripotent stem cell lines from Friedreich Ataxia patients. Stem Cell Rev 7:703–713
12. Carvajal-Vergara X, Sevilla A, D'Souza SL et al (2010) Patient-specific induced pluripotent stem-cell-derived models of LEOPARD syndrome. Nature 465:808–812
13. Raya A, Rodriguez-Piza I, Guenechea G et al (2009) Disease-corrected haematopoietic progenitors from Fanconi anaemia induced pluripotent stem cells. Nature 460:53–59
14. Maehr R, Chen S, Snitow M et al (2009) Generation of pluripotent stem cells from patients with type 1 diabetes. Proc Natl Acad Sci U S A 106:15768–15773
15. Ohnuki M, Takahashi K, Yamanaka S (2009) Generation and characterization of human induced pluripotent stem cells. Curr Protoc Stem Cell Biol Chapter 4: Unit 4A 2
16. Morita S, Kojima T, Kitamura T (2000) Plat-E: an efficient and stable system for transient packaging of retroviruses. Gene Ther 7:1063–1066
17. McMahon AP, Bradley A (1990) The Wnt-1 (int-1) proto-oncogene is required for development of a large region of the mouse brain. Cell 62:1073–1085
18. Thomson JA, Itskovitz-Eldor J, Shapiro SS et al (1998) Embryonic stem cell lines derived from human blastocysts. Science 282:1145–1147
19. Fujioka T, Yasuchika K, Nakamura Y, Nakatsuji N, Suemori H (2004) A simple and efficient cryopreservation method for primate embryonic stem cells. Int J Dev Biol 48:1149–1154
20. Nakagawa M, Koyanagi M, Tanabe K et al (2008) Generation of induced pluripotent stem cells without Myc from mouse and human fibroblasts. Nat Biotechnol 26:101–106
21. Yamamoto M, Kakihana K, Ohashi K et al (2009) Serial monitoring of T315I BCR-ABL mutation by Invader assay combined with RT-PCR. Int J Hematol 89:482–488
22. Hall JG, Eis PS, Law SM et al (2000) Sensitive detection of DNA polymorphisms by the serial invasive signal amplification reaction. Proc Natl Acad Sci U S A 97:8272–8277
23. Kadowaki T, Kadowaki H, Mori Y et al (1994) A subtype of diabetes mellitus associated with a mutation of mitochondrial DNA. N Engl J Med 330:962–968
24. Katagiri H, Asano T, Ishihara H et al (1994) Mitochondrial diabetes mellitus: prevalence and clinical characterization of diabetes due to mitochondrial tRNA(Leu(UUR)) gene mutation in Japanese patients. Diabetologia 37:504–510
25. Palo K, Mets U, Jager S, Kask P, Gall K (2000) Fluorescence intensity multiple distributions analysis: concurrent determination of diffusion times and molecular brightness. Biophys J 79:2858–2866
26. Nagano M, Katagiri S, Takahashi Y (2006) ATP content and maturational/developmental ability of bovine oocytes with various cytoplasmic morphologies. Zygote 14:299–304
27. Shiraki N, Yoshida T, Araki K et al (2008) Guided differentiation of embryonic stem cells into Pdx1-expressing regional-specific definitive endoderm. Stem Cells 26:874–885
28. Larsson SH, Charlieu JP, Miyagawa K et al (1995) Subnuclear localization of WT1 in splicing or transcription factor domains is regulated by alternative splicing. Cell 81:391–401

29. Laird PW, Zijderveld A, Linders K, Rudnicki MA, Jaenisch R, Berns A (1991) Simplified mammalian DNA isolation procedure. Nucleic Acids Res 19:4293
30. Prigione A, Fauler B, Lurz R, Lehrach H, Adjaye J (2010) The senescence-related mitochondrial/oxidative stress pathway is repressed in human induced pluripotent stem cells. Stem Cells 28:721–733
31. Lyamichev V, Mast AL, Hall JG et al (1999) Polymorphism identification and quantitative detection of genomic DNA by invasive cleavage of oligonucleotide probes. Nat Biotechnol 17:292–296
32. Mashima Y, Nagano M, Funayama T et al (2004) Rapid quantification of the heteroplasmy of mutant mitochondrial DNAs in Leber's hereditary optic neuropathy using the Invader technology. Clin Biochem 37:268–276
33. Inagaki Y, Mashima Y, Fuse N, Ohtake Y, Fujimaki T, Fukuchi T (2006) Mitochondrial DNA mutations with Leber's hereditary optic neuropathy in Japanese patients with open-angle glaucoma. Jpn J Ophthalmol 50:128–134
34. Mazunin IO, Volodko NV, Starikovskaya EB, Sukernik RI (2010) Mitochondrial genome and human mitochondrial diseases. Mol Biol 44:665–681
35. Adewumi O, Aflatoonian B, Ahrlund-Richter L et al (2007) Characterization of human embryonic stem cell lines by the International Stem Cell Initiative. Nat Biotechnol 25:803–816
36. Itskovitz-Eldor J, Schuldiner M, Karsenti D et al (2000) Differentiation of human embryonic stem cells into embryoid bodies compromising the three embryonic germ layers. Mol Med 6:88–95
37. Jenuth JP, Peterson AC, Shoubridge EA (1997) Tissue-specific selection for different mtDNA genotypes in heteroplasmic mice. Nat Genet 16:93–95
38. Ashley MV, Laipis PJ, Hauswirth WW (1989) Rapid segregation of heteroplasmic bovine mitochondria. Nucleic Acids Res 17:7325–7331
39. Laipis PJ, van de Walle MJ, Hauswirth WW (1988) Unequal partitioning of bovine mitochondrial genotypes among siblings. Proc Natl Acad Sci U S A 85:8107–8110
40. Larsson NG, Tulinius MH, Holme E et al (1992) Segregation and manifestations of the mtDNA tRNA(Lys) A–>G(8344) mutation of myoclonus epilepsy and ragged-red fibers (MERRF) syndrome. Am J Hum Genet 51:1201–1212
41. Leonard JV, Schapira AH (2000) Mitochondrial respiratory chain disorders II: neurodegenerative disorders and nuclear gene defects. Lancet 355:389–394
42. Chou BK, Mali P, Huang X et al (2011) Efficient human iPS cell derivation by a non-integrating plasmid from blood cells with unique epigenetic and gene expression signatures. Cell Res 21:518–529
43. Williams RS, Salmons S, Newsholme EA, Kaufman RE, Mellor J (1986) Regulation of nuclear and mitochondrial gene expression by contractile activity in skeletal muscle. J Biol Chem 261:376–380
44. Cho YM, Kwon S, Pak YK et al (2006) Dynamic changes in mitochondrial biogenesis and antioxidant enzymes during the spontaneous differentiation of human embryonic stem cells. Biochem Biophys Res Commun 348:1472–1478
45. Facucho-Oliveira JM, Alderson J, Spikings EC, Egginton S, St John JC (2007) Mitochondrial DNA replication during differentiation of murine embryonic stem cells. J Cell Sci 120:4025–4034
46. Harvey A, Gibson T, Lonergan T, Brenner C (2010) Dynamic regulation of mitochondrial function in preimplantation embryos and embryonic stem cells. Mitochondrion 11:829–838
47. St John JC, Facucho-Oliveira J, Jiang Y, Kelly R, Salah R (2010) Mitochondrial DNA transmission, replication and inheritance: a journey from the gamete through the embryo and into offspring and embryonic stem cells. Hum Reprod Update 16:488–509
48. Wong LJ, Perng CL, Hsu CH et al (2003) Compensatory amplification of mtDNA in a patient with a novel deletion/duplication and high mutant load. J Med Genet 40:e125
49. Kim K, Lecordier A, Bowman LH (1995) Both nuclear and mitochondrial cytochrome c oxidase mRNA levels increase dramatically during mouse postnatal development. Biochem J 306:353–358
50. Ostronoff LK, Izquierdo JM, Enriquez JA, Montoya J, Cuezva JM (1996) Transient activation of mitochondrial translation regulates the expression of the mitochondrial genome during mammalian mitochondrial differentiation. Biochem J 316:183–191

BRAIN RESEARCH 1435 (2012) 154–166

Available online at www.sciencedirect.com

SciVerse ScienceDirect

www.elsevier.com/locate/brainres

BRAIN RESEARCH

Research Report

Kcna1-mutant rats dominantly display myokymia, neuromyotonia and spontaneous epileptic seizures

Saeko Ishida[a], *Yu Sakamoto*[b], *Takeshi Nishio*[c], *Stéphanie Baulac*[a,d,e], *Mitsuru Kuwamura*[f], *Yukihiro Ohno*[g], *Akiko Takizawa*[a], *Shuji Kaneko*[b], *Tadao Serikawa*[a], *Tomoji Mashimo*[a,*]

[a]*Institute of Laboratory animals, Graduate School of Medicine, Kyoto University, Kyoto 606-8501, Japan*
[b]*Department of Molecular Pharmacology, Graduate School of Pharmaceutical Sciences, Kyoto University, Kyoto 606-8501, Japan*
[c]*Department of Integrative Brain Science, Graduate School of Medicine, Kyoto University, Kyoto 606-8501, Japan*
[d]*Inserm U975, CRICM, Paris F-75013, France*
[e]*Université Pierre & Marie Curie-Paris 6, UMR_S975, Paris F-75013, France*
[f]*Laboratory of Veterinary Pathology, Osaka Prefecture University, Izumisano, Osaka 598-8531, Japan*
[g]*Laboratory of Pharmacology, Osaka University of Pharmaceutical Sciences, Takatsuki 569-1094, Japan*

ARTICLE INFO

Article history:
Accepted 8 November 2011
Available online 13 November 2011

Keywords:
Episodic ataxia type 1 (EA1)
Animal model
Phenotype-driven ENU mutagenesis
Voltage-gated potassium channel shaker-related subfamily member 1 (Kcna1)
Voltage-sensor domain S4
Dominant-negative effect

ABSTRACT

Mutations in the *KCNA1* gene, which encodes for the α subunit of the voltage-gated potassium channel Kv1.1, cause episodic ataxia type 1 (EA1). EA1 is a dominant human neurological disorder characterized by variable phenotypes of brief episodes of ataxia, myokymia, neuromyotonia, and associated epilepsy. Animal models for EA1 include *Kcna1*-deficient mice, which recessively display severe seizures and die prematurely, and V408A-knock-in mice, which dominantly exhibit stress-induced loss of motor coordination. In the present study, we have identified an N-ethyl-N-nitrosourea-mutagenized rat, named autosomal dominant myokymia and seizures (ADMS), with a missense mutation (S309T) in the voltage-sensor domain, S4, of the *Kcna1* gene. ADMS rats dominantly exhibited myokymia, neuromyotonia and generalized tonic–clonic seizures. They also showed cold stress-induced tremor, neuromyotonia, and motor incoordination. Expression studies of homomeric and heteromeric Kv1.1 channels in HEK cells and *Xenopus* oocytes, showed that, although S309T channels are transferred to the cell membrane surface, they remained non-functional in terms of their biophysical properties, suggesting a dominant-negative effect of the S309T mutation on potassium channel function. ADMS rats provide a new model, distinct from previously reported mouse models, for studying the diverse functions of Kv1.1 in vivo, as well as for understanding the pathology of EA1.

1. Introduction

Episodic ataxia type 1 (EA1) is an autosomal dominant neurological disorder, with an age of onset in childhood or early adolescence. EA1 is characterized by myokymia (involuntary quivering or rippling of muscle bundles), and episodic attacks of ataxia (loss of motor coordination and balance with spastic contractions of the skeletal muscles) (Pessia and Hanna, 1993;

* *Corresponding author at:* Institute of Laboratory Animals, Graduate School of Medicine, Kyoto University, Yoshidakonoe-cho, Sakyo-ku, Kyoto 606-8501, Japan. Fax: +81 75 753 4409.
E-mail address: tmashimo@anim.med.kyoto-u.ac.jp (T. Mashimo).

0006-8993/$ – see front matter © 2011 Elsevier B.V. All rights reserved.
doi:10.1016/j.brainres.2011.11.023

Rajakulendran et al., 2007). EA1 is also associated with an increased incidence of epilepsy (Zuberi et al., 1999) and hypomagnesaemia (Glaudemans et al., 2009a). Since clinical manifestations of EA1 are widely variable, with respect to the severity of ataxia and myokymia, and the occurrence of neuromyotonia (muscle stiffness, twitching, and fasciculation), and epilepsy (Eunson et al., 2000; Gilbert et al., 2011; Poujois et al., 2006; Tomlinson et al., 2010), clinical diagnosis is based on genetic testing of *KCNA1*. *KCNA1* encodes the α subunit of the voltage-gated potassium channel, Kv1.1, and is the only known gene associated with EA1 (Browne et al., 1994). The *KCNA1* mutations reported in EA1 patients are predominantly missense mutations that are distributed throughout the gene. However, a nonsense mutation has also been identified at the C-terminal end of *KCNA1* (Eunson et al., 2000). The phenotypic variability of EA1 may be associated with the distinct mutations of *KCNA1*; however, phenotypic differences are present not only among families, but also among individuals carrying the same mutation within the same family, suggesting the interplay of modifier genes and/or non-genetic factors (Gilbert et al., 2011). Because of this high degree of intra- and interfamilial genetic and environmental variability, determining genotype–phenotype correlations in humans is problematic. Animal models can greatly improve our understanding of human disease pathogenesis under the control of specific genetic and environmental conditions.

N-ethyl-N-nitrosourea (ENU) mutagenesis has been widely used to generate animal models of human diseases by two complementary approaches, forward and reverse genetics. A reverse genetics, or gene-driven approach (gene to phenotype), screens for mutations within a gene of interest, in ENU-mutagenized animals, enabling subsequent investigation of gene function. For the reverse genetics approach, we have generated a large repository of ENU-mutagenized rats, the Kyoto University Rat Mutant Archive (KURMA: http://www.anim.med.kyoto-u.ac.jp/enu) (Mashimo et al., 2008). KURMA contains genomic DNA and frozen sperm from 10,000 ENU-mutagenized G1 rats, and will be used to screen mutations of targeted genes using a high-throughput screening assay based on the Mu-transposition reaction (MuT-POWER). Subsequent recovery of corresponding sperm by intracytoplasmic sperm injection (ICSI), will establish gene-targeted rat models of human diseases (Mashimo et al., 2010; Yoshimi et al., 2009). Alternatively, a forward genetics, or phenotype-driven approach (phenotype to gene), involves screening ENU-mutagenized animals for abnormal phenotypes, and then mapping the casual mutation. The forward genetic approach allows mutagenized animals expressing symptoms of interest to be identified, and may offer new insight into disease pathogenesis.

In this study, we used a forward genetic screen on ENU-mutagenized G1 rats to identify neurological phenotypes. We identified a rat exhibiting persistent myokymia, neuromyotonia, and spontaneous epileptic seizures, subsequently named autosomal-dominant myokymia and seizures (ADMS) rats. Positional cloning identified a missense mutation (S309T), in the *Kcna1* gene, located in the voltage-sensor segment (S4), of Kv1.1. The S309T mutation is in close proximity to the L305F mutation previously identified in a French EA1 family, exhibiting brief episodes of ataxia in early childhood and progressive development of chronic neuromyotonia (Poujois et al., 2006). Thus ADMS rats provide a new model of EA1, which are genetically and phenotypically different from previously reported mouse models.

2. Results

2.1. *An ENU-mutagenized rat exhibiting twitching and spontaneous seizures*

In the first generation of the progeny (G1) from an ENU-injected F344 male, one female exhibited abnormal behaviours, characterized by muscle twitching and spontaneous convulsive seizures. To determine the mode of inheritance, this "affected" G1 female was backcrossed with an F344 male. Of the backcross progeny, 16 (53.3%) rats exhibited the abnormal behaviours, with 14 (46.7%) rats phenotypically normal. Both twitching and seizure behaviours always co-segregated, and there were no gender differences. Further backcrossing of affected males to F344 females, for ten generations (N10), resulted in approximately 50% of the progeny affected and 50% unaffected in each generation. This pattern of inheritance, suggests that on an F344 genetic background, the abnormal behaviours of muscle twitching and seizures, are inherited in an autosomal dominant pattern. Thus, we named this inbred strain of rats, autosomal-dominant myokymia and seizures (ADMS).

Interestingly, compared with F344 rats, ADMS rats showed slightly but significantly increased body weight from 10 to 13 weeks of age (Fig. 1A), that coincided with severe twitching behaviour. Physically, the ADMS rats appeared swollen, and were not obese. From 16 weeks of age, the body weight of ADMS rats significantly decreased, compared with F344 rats, coinciding with severe periodic seizures. By 30 weeks of age, 84% of ADMS rats had died. In contrast, no F344 or ADMS rats on a BN background, died at this age (Fig. 1B). This increased mortality in ADMS rats coincided with a reduced body weight and increased number of convulsive seizures. Postmortem examination showed no obvious morphological abnormalities in any tissues examined from ADMS rats.

2.2. *Neuromyotonia and myokymia in ADMS rats*

ADMS rats began to display muscle twitching from 6 weeks of age, typically characterized by coordinated muscle contraction of the eyelid, the neck, and the extremities (Fig. 1C; Supplementary Video 1). Startle responses, twitching behaviour in response to sudden acoustic stimuli such as clapping hands, was also evident (Fig. 1D). The number of twitches increased with age until 18 weeks, then decreased, coinciding with loss of mobility, reduced body weight and increased convulsive seizures in the rats. To further characterize muscle twitching in ADMS rats, we used EMG to record muscle activity from fore and hind limbs (Fig. 1D). Spontaneous myoclonic discharges, correlating with muscle twitching, were detected from the hind limbs. Large spikes were recorded from both fore and hind limbs in response to sound stimulation, reflecting myoclonic startle responses. Importantly, EMG recordings from fore limbs

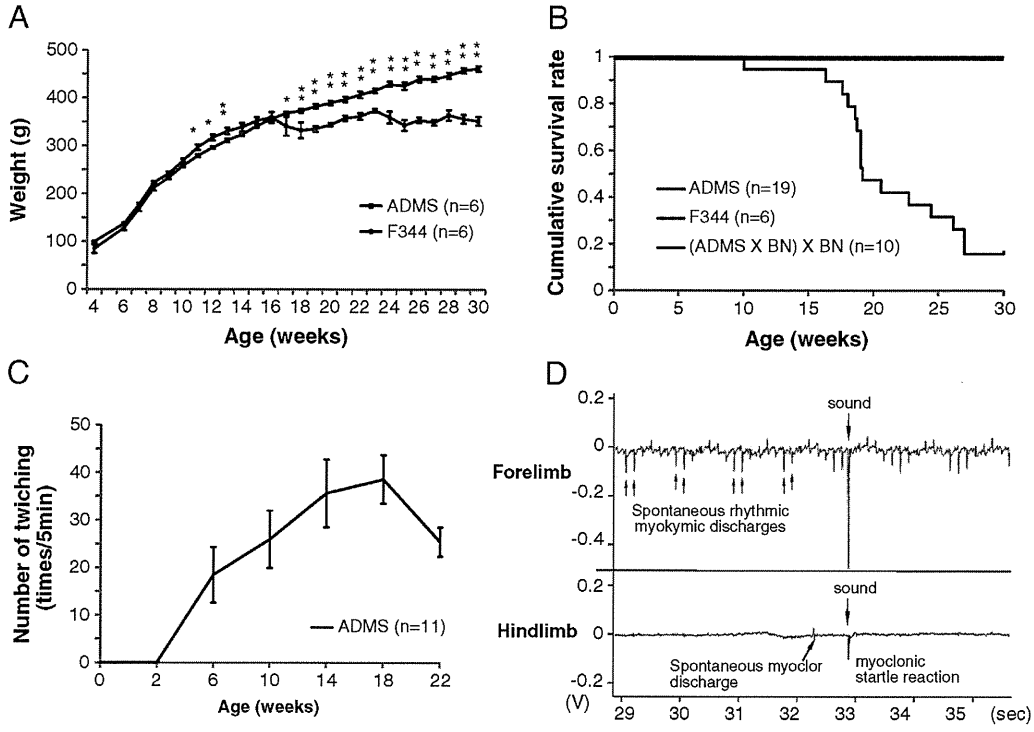

Fig. 1 – Gross and myokymic phenotypes in ADMS rats. (A) Comparison of body weight between ADMS (n=6) and F344 (n=6) rats. ADMS rats show increased body weight from 10 weeks of age, which is then reduced, in conjunction with the severe convulsive seizures from 18 weeks of age. Error bars indicate SEM. Unpaired student's t-test: *p<0.05, **p<0.01. (B) Kaplan–Meier survival curves of ADMS (n=19), F344 (n=6) rats, and (ADMS×BN)×BN backcross progeny (n=10). By 30 weeks of age, 84% of ADMS rats had died. (C) Twitching behaviours appeared from 6 weeks of age and peaked at 18 weeks of age in ADMS rats (n=11). Error bars indicate SEM. (D) Electromyogram (EMG) recording of forelimb and hindlimb muscles during the interictal period in 16-week-old ADMS rats. A spontaneous myoclonic discharge was detected from the hindlimb, as well as a myoclonic startle reaction in response to a sound stimulus. Spontaneous rhythmic myokymic discharges (7 Hz) were detected from the forelimb.

also showed rhythmic multiple discharges with an intra-burst frequency of 7 Hz. This firing pattern is similar to that observed in human myokymia.

2.3. *Spontaneous convulsive seizures in ADMS rats*

ADMS rats exhibited spontaneous convulsive seizures from 10 weeks of age (Fig. 2A). Occurrence of seizures was aggravated during cage changing or animal handling. Seizure onset was observed in all ADMS rats (n=11) by 16 weeks of age. The average number of seizures significantly increased with age until 20 weeks of age (Fig. 2A), while the mean duration of each seizure did not increase (Fig. 2B). The typical seizure phenotype encompassed four stages: (i) initial sudden falling down, (ii) secondly jerking of the entire body or the extremities as clonic phase, occasionally with a tonic phase with stiffening of the entire body, (iii) immobility, and (iv) rearing with muscle twitching (Fig. 2C; Supplementary Video 2). Motor automatisms, such as repetitive chewing, occasionally occurred during the seizure. Cortical and hippocampal EEG recordings identified four characteristic EEG patterns corresponding to the four stages of the seizure phenotype. First, aberrant large spike activity associated with falling-down behaviour (i). Second, low-voltage fast wave discharges detected during the tonic stage, and spike-and-wave discharges (2 Hz) detected during the clonic convulsive stage (ii). These discharges terminated abruptly, followed by fast spikes with low to high voltages in the freezing stage (iii). Finally, polyspike and large wave complexes (1–3 Hz) during the rearing stage (iv). Although cortical and hippocampal EEG recordings were generally synchronized, ictal epileptic activities in the hippocampus tended to precede cortical discharges, specifically at the onset of seizure ((i) initial sudden falling), and/or during the transition stage between freezing (iii) and rearing (iv). The behavioural phenotypes and abnormal discharge patterns in ADMS rats are similar to other rodent models of temporal lobe epilepsy (Rho et al., 1999; Wenzel et al., 2007). These spontaneous convulsive seizures and the twitching phenotypes were significantly prevented 30 min after the administration of carbamazepine (CBZ) in ADMS rats (n=5) (Figs. 2D, E). Histopathological analysis of ADMS rats at 16–19 weeks of age revealed no major abnormalities in haematoxylin staining of the brain (Supplementary Fig. 1).

2.4. *Identification of a Kcna1 S309T mutation*

We crossed ADMS females to BN males, a rat strain suitable for genetic mapping studies, because of their distinct genetic background. We obtained eight F1 progeny exhibiting the

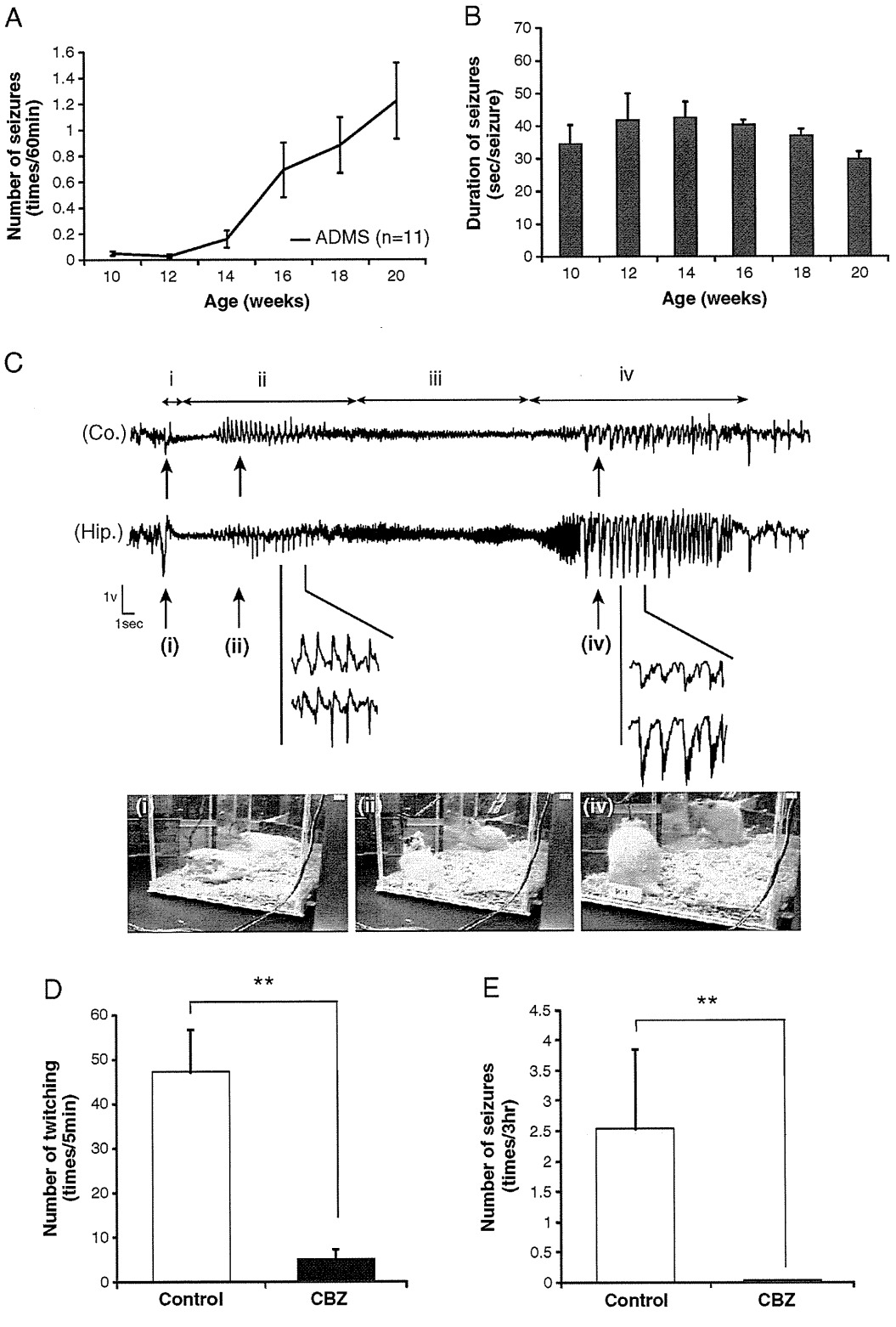

Fig. 2 – Spontaneous epileptic seizures in ADMS rats. (A) Convulsive seizures started from 10 weeks of age and increased in number, peaking at 20 weeks of age in ADMS rats (n=11). Error bars indicate SEM. (B) The mean duration of seizures did not differ between ages. Unpaired student's t-test: $p>0.05$. (C) Cortical (Co.) and hippocampal (Hip.) electroencephalogram (EEG) recorded from an ADMS rat at 16 weeks of age. Although the discharges occurred synchronously in both cortex and hippocampus, the amplitude was higher in hippocampus than in cortex. Behavioural patterns were correlated with EEG events. i: tonic attack; ii: clonus of the limbs; iii: immobility; and iv: rearing with chewing gesture. Photographs show characteristic postures in stages i, ii and iv. (D) The spontaneous convulsive seizures in ADMS rats (n=5) were prevented by the administration of carbamazepine (CBZ). (E) Numbers of the twitching behaviours in ADMS rats (n=5) were significantly decreased by CBZ. Paired student's t-test: $^{**}p<0.01$.

same abnormal behaviours as the ADMS rats, albeit with a slightly delayed onset. Muscle twitching was observed from 10 to 12 weeks of age, compared with 6 weeks in ADMS rats, while spontaneous convulsive seizures were not evident until 20–30 weeks of age in four animals, with the remaining four animals not presenting with seizures until 40 weeks, suggesting modifier gene(s) are associated with the onset of seizures. Further breeding, generated 180 (ADMS×BN)×BN

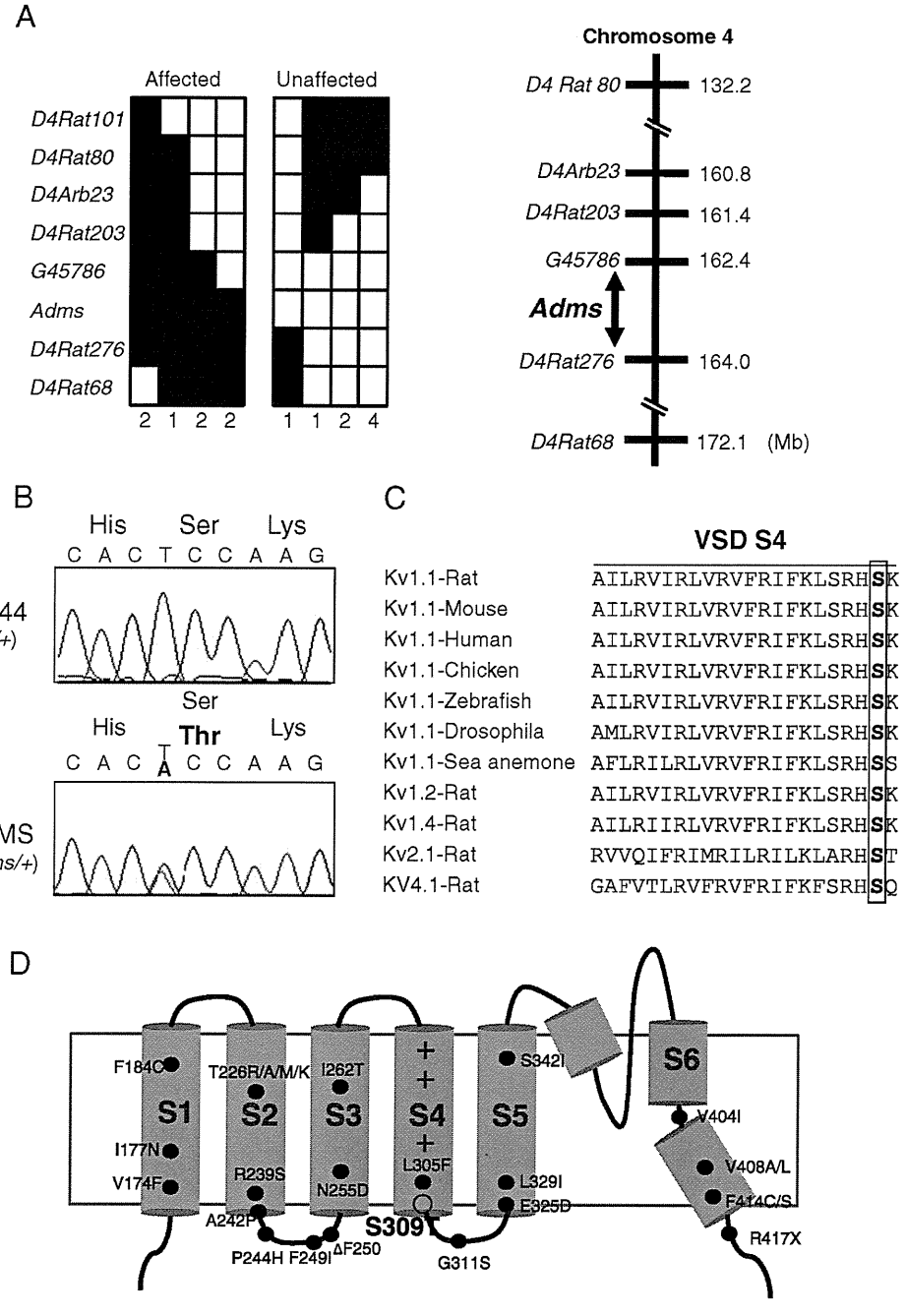

Fig. 3 – Identification of *Adms* mutation. (A) (Left) Distribution of haplotypes in (ADMS×BN)×BN backcross progeny, determined using SSLP markers from rat chromosome 4. White boxes represent BN homozygous alleles or 'unaffected' for *Adms*. Black boxes represent F344-derived heterozygotes or 'affected' alleles. Numbers of the backcross progeny are depicted at the bottom of the haplotypes. (Right) *Adms* was mapped to a 1.6-Mb region between *G45786* and *D4Rat276*. (B) Sequencing analysis in F344 (upper) and ADMS (lower) rats revealed a nucleotide change from T to A (arrowhead) located at position 925 of the *Kcna1* gene. The mutation results in an amino acid substitution of serine (Ser) with threonine (Thr) at codon 309 of the KCNA1 protein. (C) Amino acid sequence alignment of the voltage-sensor domain S4 of KCNA1 in several species and between KCNA families. The S309T amino acid substitution (boxed) is located in a region highly conserved among species and within the KCNA family. (D) Schematic representation of the Kv1.1 subunit. Black circles represent the positions of the EA1 mutations thus far reported and a white circle represents the rat *Adms* mutation.

backcross progeny, with 87 rats expressing the twitching phenotype at 10–14 weeks of age, and seizure activity from 20 weeks of age.

Genome-wide scanning using 121 SSLP markers mapped the *Adms* locus to a 1.6-Mb genomic region, between markers G45786 and D4Rat276 on Chr 4 (Fig. 3A). Eighteen known or predicted genes within the *Adms* region were obtained from the Ensembl database (http://www.ensembl.org). Among them were the voltage-gated potassium channel families, *Kcna1*, *Kcna5*, and *Kcna6*, that we deemed to be good candidates, based on their functional ability to regulate membrane potential, neuronal excitability, and nerve signalling (Johnston et al., 2010; Wulff et al., 2009). In particular, the behavioural phenotypes of ADMS rats were similar to those of *Kcna1*-deficient mice (Smart et al., 1998), and to the symptoms reported in human EA1 (Pessia and Hanna, 1993; Rajakulendran et al., 2007). We compared the sequences of *Kcna1*, *Kcna5*, and *Kcna6* between F344 and ADMS rats, and identified a T-to-A mutation at nucleotide 925 of the *Kcna1* gene, but no mutations in *Kcna5* and *Kcna6* genes (Fig. 3B). The T925A mutation of *Kcna1* results in a substitution of serine for threonine at residue 309, which is located in the voltage sensor segment, S4, of Kv1.1. This residue is highly conserved among species and other potassium channel family genes (Fig. 3C). To date, more than 20 *KCNA1* mutations have been reported in EA1 patients (Bretschneider et al., 1999; Browne et al., 1994; Browne et al., 1995; Chen et al., 2007; Comu et al., 1996; Demos et al., 2009; Eunson et al., 2000; Glaudemans et al., 2009b; Graves et al., 2010; Imbrici et al., 2008; Kinali et al., 2004; Klein et al., 2004; Knight et al., 2000; Lee et al., 2004; Poujois et al., 2006; Scheffer et al., 1998; Shook et al., 2008; Zerr et al., 1998; Zuberi et al., 1999) (Fig. 3D). Interestingly, the *KCNA1* missense mutation L305F, which is closely located to S309T in the S4 segment, was reported in an EA1 family uniquely exhibiting brief episodes of cerebellar ataxia in early childhood and progressive development of chronic neuromyotonia with muscle rippling and hypertrophy (Poujois et al., 2006).

2.5. *Premature death of homozygous S309T rats*

To investigate the effect of the homozygous mutation of *Kcna1* S309T, we crossed N10 heterozygous ADMS males and females. The behaviour and appearance of homozygous S309T/S309T rats at birth did not differ from those of heterozygous S309T/+ and WT+/+ littermates. Western blot analysis showed that the expression level of endogenous KCNA1 protein in the brain did not differ between homozygous, heterozygous and WT littermate rats (Supplementary Fig. 2). However, from postnatal day 14, development of the homozygous rats was dramatically impaired and body weight significantly decreased compared with heterozygous and WT littermates (Fig. 4A). In conjunction with reduced body weight, the homozygous rats showed tremors, motor incoordination, mainly caused by extension of hind limbs, and spontaneous convulsive seizures (Supplementary Video 3). These phenotypes progressively worsen with age. Homozygous pups became inactive except during seizures, and usually remained isolated from their mother. All homozygous rats died prematurely with a mean lifetime of 16 days (Fig. 4B).

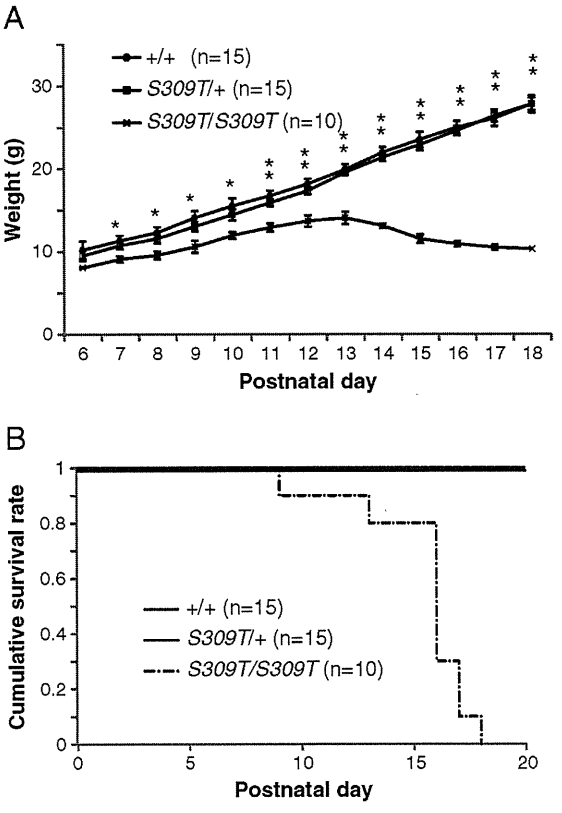

Fig. 4 – Lethality of homozygous S309T rats. (A) From postnatal (P) 7 days, the body weight of homozygous S309T/S309T rats (n=10) was significantly reduced compared with heterozygous S309T/+ (n=15) and WT+/+ (n=15) rats. Error bars indicate SEM. Unpaired student's t-test: *p<0.05, **p<0.01. (B) Kaplan–Meier survival curves of homozygous S309T/S309T (n=10), heterozygous S309T/+ (n=15) and WT+/+ (n=15) rats. All homozygous rats had died by P18.

No homozygous rats survived beyond postnatal day 18, while neither heterozygous or WT littermates died at this age. Postmortem examination of homozygous rats detected an absence of stomach contents, suggesting early mortality might result from feeding failure partially caused by the severe behavioural phenotypes.

2.6. *Motor incoordination by cold-swim tests*

To examine whether ADMS rats show cold-swim induced neuromyotonia and motor incoordination that were recognized in *Kcna1*-deficient mice (Zhou et al., 1998), we forced rats to swim in a tank filled with either warm (38 °C) or cold (17 °C) water. We used 5-week-old ADMS rats that have never exhibited muscle twitching or spontaneous seizures. In warm water, there was no behavioural difference between ADMS and WT rats during 2-min swimming in the tank and subsequent 5-min observation on a dry platform at room temperature. In cold water however, there was an observable difference between ADMS and WT rats. Toward the end of the 2-min swimming period, ADMS rats had difficulties maintaining axial orientation and